Improved daily $PM_{2.5}$ estimates in India reveal inequalities in recent enhancement of air quality

Ayako Kawano [1,*], Makoto Kelp [2], Minghao Qiu [2,3], Kirat Singh [1], Eeshan Chaturvedi [1], Inés Azevedo [4], Marshall Burke[5,6,7]

1 Emmett Interdisciplinary Program in Environment and Resources, Stanford University, Stanford, CA, USA

2 Department of Earth System Science, Stanford University, Stanford, CA, USA

3 Center for Innovation in Global Health, Stanford University, Stanford, CA, USA

4 Department of Energy Science and Engineering, Stanford University, Stanford, CA, USA

5 Doerr School of Sustainability, Stanford University, Stanford, CA, USA

6 Center on Food Security and the Environment, Stanford University, Stanford, CA, USA

7 National Bureau of Economic Research, Cambridge, MA, USA

***** To whom correspondence should be addressed. E-mail: akawano@stanford.edu

Abstract

Poor ambient air quality represents a substantial threat to public health globally. However, accurate measurement of air quality remains challenging in many parts of the world, including in populous countries like India, where ground monitors are scarce yet exposure and health burdens are expected to be high. This lack of precise measurement impedes understanding of how pollution exposure changes over time and varies across different populations, and inhibits monitoring of interventions to improve air quality. Here we develop open-source daily fine particulate matter ($PM_{2.5}$) datasets at a 10 km resolution for India from 2005 to 2023, using a region-specific two-stage machine learning model carefully validated on held-out monitor data that it was not trained on. Our model demonstrates robust out-of-sample performance, substantially outperforming existing publicly-available monthly $PM_{2.5}$ datasets. We use model output to analyze long-term air quality trends, finding that $PM_{2.5}$ increased across most of the country until around 2016 and then began to decline thereafter, partially driven by favorable meteorology in southern India. Importantly, recent $PM_{2.5}$ reductions were substantially larger in wealthier areas, albeit from a higher initial level, but we find no evidence that the recently-adopted National Clean Air Program has improved air quality in targeted urban areas to date. Our results highlight the urgency of air quality control policies that effectively target both lower and higher socioeconomic groups. To further enhance air quality monitoring across populations in India and other countries, we use model output to propose locations where new ground monitors should be installed in India, and examine the adaptability of our method to other settings with scarce ground monitoring data.

INTRODUCTION

Exposure to ambient fine particulate matter ($PM_{2.5}$) is a recognized global health concern. India, with its large population and high average pollution levels, bears a substantial share of the global health burden from poor air quality (*1*). Importantly, the health burden of air pollution often varies across individuals and groups with different socio-economic status, due to differences in pollution concentrations, as well as the increased sensitivity of health outcomes to pollution exposure in lower-income communities (*2*). While these disparities in air pollution exposure across wealth groups have been well documented in high-income countries (*2–4*), evidence from low- and middle-income countries remains limited, primarily due to sparse air quality monitoring networks, especially in rural areas where large proportions of the population live, along with a lack of data on wealth at fine temporal and spatial resolutions (*3*). A population-scale understanding of trends and exposure to air pollution, including in wealthier and poorer areas of low- and middle-income countries such as India, is urgently needed to understand and address the impacts of air pollution exposure across diverse socioeconomic groups.

Despite recent efforts in expanding the air quality monitoring network in the country, India still faces a great challenge in comprehensive measurement of surface air quality. The Central Pollution Control Board (CPCB) initiated the National Ambient Air Quality Monitoring (NAAQM) Network in 1984, beginning with the installation of manual monitoring stations, where pollutants are subsequently analyzed in the laboratory (*5*). Continuous Ambient Air Quality Monitoring System (CAAQMS), which provides real-time data, was first introduced in Delhi in 2006 and expanded to other cities after 2016 (*6*). The CPCB manages 883 manual stations and 438 continuous monitoring stations as of February 2023 (*7*), and this relatively small number of monitors results in a much higher ratio of population to continuous air quality monitors in India (3.2 million people per monitor) compared to the US (0.1 - 0.5 million people per monitor (*8*)), EU (0.1 million people per monitor (*9*)), and China (0.9 million people per monitor (*10*)). Moreover, most current CAAQMS monitors are situated in populous urban areas where wealthier people reside (Figure S1). The government of India has committed to expanding the CAAQMS network up to 1,000 monitors under the National Clean Air Program (NCAP), which started in 2019 (*11*); however, the placement of these additional continuous monitors remains an ongoing policy question, and it is uncertain whether environmental inequalities are considered or prioritized in determining their locations.

Previous population-based studies (*12*, *13*) have explored the disproportionate exposure to air pollution and associated health impacts in low- and middle-income countries, including India, by utilizing publicly available modeled $PM_{2.5}$ estimates. One widely utilized dataset for such analyses is global monthly estimates of $PM_{2.5}$, integrating satellite retrievals of Aerosol Optical Depth (AOD), atmospheric chemical transport models, and ground-based measurements (*14*). While this dataset has proven valuable on a global scale, significant uncertainties persist in regions with limited ground monitoring stations, including India (*14*). Furthermore, it is likely that region-specific models could substantially outperform global models in measuring air pollution in a target region of interest, as has been found in the US (*15*).

In addition to the uncertainty in estimating $PM_{2.5}$ concentrations, the coarse temporal resolution of existing datasets (i.e monthly) hinders the assessment of short-term health effects of $PM_{2.5}$, such as effects on all-cause, respiratory, and cardiovascular mortality (*16–23*). Furthermore, monthly estimates fail to capture short-term spikes in $PM_{2.5}$ emissions at the local to regional scales, such as crop residue burning. Acknowledging the need for a dataset with finer temporal resolution, a growing number of studies (*24–26*) have worked on developing daily $PM_{2.5}$ estimates for India. However, their datasets are not publicly accessible, inhibiting their use by both researchers and a host of governmental and non-governmental actors. Using up-to-date data to comprehensively characterize temporal and spatial trends in exposure, and potential differences in exposure by socioeconomic status, is also critical for understanding how and why exposures are changing and who is being most impacted.

Here we develop an open-source daily $PM_{2.5}$ dataset at 10 km resolution for India over 2005 - 2023 by training a machine learning model to predict the limited available ground monitor data with abundant data from remote sensing. Previous studies have employed machine learning algorithms, such as neural networks, random forest, and extreme gradient boosting (XGBoost), to predict ambient $PM_{2.5}$ concentrations (*27*, *28*). Due to the theoretical relationship between satellite AOD and surface $PM_{2.5}$ (*27*, *29*), satellite-derived AOD has long been a key input feature used to train machine learning models for air pollution measurement, often in combination with data on meteorology, land cover, elevation, and population density (*27*, *28*). However, the substantial amount of missing AOD values due to clouds and bright surfaces has posed challenges in reducing predictive errors when estimating $PM_{2.5}$ concentrations through machine learning methods. (*27*, *30*). To address this issue, a common recent approach involves imputing missing data in AOD observations using machine learning methods (*24*, *25*, *31*). Additionally, new satellite sensors provide alternative input features for predicting $PM_{2.5}$ concentrations without relying on AOD, such as data from the Sentinel-5 Precursor (Sentinel-5P) mission's TROPOspheric Monitoring Instrument (TROPOMI) (*30*, *32*, *33*). However, it is still unknown how much the predictive performance differs between satellite-derived AOD and TROPOMI-based features in estimating $PM_{2.5}$ concentrations, and whether the two sources of data independently add value in predicting surface $PM_{2.5}$ concentrations.

To take advantage of both the longer available time series of AOD data and information from these newer sensors, we use available ground monitoring data to train two separate models, which we term as the "Full model" and the "AOD model". The Full model combines both Moderate Resolution Imaging Spectroradiometer (MODIS) AOD (*34*) and TROPOMI satellite inputs (nitrogen dioxide (NO_2) (*35*) and carbon monoxide (CO) (*36*) along with other inputs, Figure S2 and

Materials and Methods) and is trained on data from July 2018, when TROPOMI features become available, through September 2023 (Figure S2, S3). It produces daily estimates across the country for the period corresponding to its training period. The AOD model retains all inputs except TROPOMI and trains on data beginning January 2013 (Figure S2, S3), and is used to generate daily predictions from January 2005 to September 2023. In both the Full and AOD models, we first fill the missing satellite observations in either AOD or TROPOMI using a separate machine learning model (see Materials and Methods). The gap-filled estimates are then combined with the other features in a second-stage model that predicts surface $PM_{2.5}$ concentrations as measured by CAAQMS monitors (n = 435) (Figure S4).

Critically, and in contrast to related work(*24*, *25*), our second stage model is evaluated using spatial cross-validation (CV) (Figure S5) – i.e. we evaluate model predictions on entirely held-out monitoring stations – rather than conventional random CV, in which a given station can contribute data to both the training and test sets. This more challenging performance metric is meant to ensure that the model generalizes to locations where it has no data to train, which is most of India. Using spatial CV, we then calculate two performance metrics: (1) the total R^2, or the percent of variation in observed $PM_{2.5}$ explained by model predictions, as well as (2) the "within" R^2, or the percent of variation in observed $PM_{2.5}$ explained by predictions after accounting for both differences in average $PM_{2.5}$ across locations as well as seasonal differences in $PM_{2.5}$ within a given location. In essence, the within R^2 meausres whether our model can predict daily $PM_{2.5}$ anomalies relative to location- and season-specific averages, rather than simply predict spatial or seasonal patterns correctly. This "within" variation is often exploited in studies of the impact of air pollution of health and related societal outcomes, and thus is a highly-relevant, if rarely-reported, performance metric.

We utilize model-derived predictions to better characterize nationwide air quality trends, including inequalities in $PM_{2.5}$ exposure by region and wealth level, and to identify locations with extreme $PM_{2.5}$ concentrations. We then use our predictions, along with emissions inventories, meteorological data, and administrative data on national air quality programs, to better understand why pollution concentrations are changing. This includes, to our knowledge, the first evaluation of whether the recently-adopted National Clean Air Program (NCAP) is improving air quality in targeted areas relative to a comparable set of non-targeted areas. Subsequently, to address current gaps in the air quality monitoring network in India, we use our $PM_{2.5}$ estimates and compressed sensing methods (*37*) (see Materials and Methods) to propose where additional air quality monitors could be installed to maximize the ability of the ground network to capture variability in surface air pollution across both wealthier and lower-wealth regions. Finally, we explore how our approach could supplement limited monitor data in other low- and middle-income countries by investigating the number of air quality monitors required to achieve reasonable model performance using our machine learning approach.

RESULTS

Model performance

The spatial out-of-sample performance of the Full model, assessed across daily $PM_{2.5}$ observations in the held-out fold, yielded an R^2 of 0.68 (Figure 1A). Importantly, our model effectively predicts local and temporal $PM_{2.5}$ variation rather than average differences in $PM_{2.5}$ concentrations between locations, months, or years (within $R^2 = 0.49$) (Figure 1A). The AOD model demonstrated a comparable performance, with an R^2 of 0.64 and within R^2 of 0.45 (Figure S6). When aggregated at the monthly level, our model substantially outperforms the existing publicly-available monthly $PM_{2.5}$ dataset (*14*) when evaluated on Indian monitoring data, with an R^2 of 0.74 and within R^2 of 0.52 (Figure S7). Examining location-specific performance, the out-of-sample within R^2 for each 10 km grid suggests that the northwest, northeast, and south regions exhibit higher within R^2 (Figure 1B) (for the performance of AOD model, Figure S8). We find that these differences in regional performance are substantially driven by differences in the level and variance of $PM_{2.5}$ concentrations at the station level and the number of air quality monitors within 100 km (Figure S9); performance is much higher in locations with higher and more variable $PM_{2.5}$ and with more stations nearby, consistent with the model having an easier time learning patterns in these higher signal-to-noise areas.

To further evaluate the out-of-sample spatio-temporal performance of the Full model in different locations, the daily variations in the observed and predicted $PM_{2.5}$ are compared in five mega-cities in India: New Delhi, Mumbai, Bangalore, Chennai, and Kolkata (Figure 1C) (for the AOD model, Figure S10). These five mega-cities are selected based on their population size, with each being among the most populated cities in India (*38*). Among these cities, New Delhi shows the highest performance, R^2 of 0.83 and within R^2 of 0.69 (Figure 1C). This aligns with our prior analysis on model performance because New Delhi demonstrates dense CAAQMS network and significant variance in $PM_{2.5}$ concentrations (Figure S11), primarily driven by distinct seasonal patterns caused by meteorological conditions restricting pollutant dispersion and the concurrent operation of brick manufacturing around Delhi during winter. (*39*, *40*).

We observe variations in model performance driven by distinct seasonality throughout the year across the winter (December to February), spring (March), summer (April to May), monsoon (June to September), and post-monsoon (October to November). Both the Full and AOD models demonstrate strong performance in dry seasons (winter and post-monsoon) (Figure S12). However, their performance declines during spring, summer, and monsoon periods (Figure S12), likely the result of clouds introducing noise in the remotely-sensed input features during these wetter periods.

We find consistent results in sensitivity analysis, yielding an R^2 of 0.62 and within R^2 of 0.44 when the Full model underwent training and testing on significantly larger blocks based on latitude

(Figure S13, S14), which helps rule out the possibility that our high model performance is simply being driven by auto-correlation between nearby train and test locations. When evaluated using 10-fold random CV rather than spatial CV, our model showed notably higher performance (R^2 of 0.85 and within R^2 of 0.72) (Figure S15), highlighting the potential of random CV to overstate model performance on critical real-world applications (i.e. accurately predicting variation in locations where the model was not trained).

Furthermore, as a result of model comparison using the same sets of training and test data from July 10, 2018, to September 30, 2023, the Full model reported the highest performance, achieving an R^2 of 0.67 and within R^2 of 0.55 (Figure S16). The TROPOMI model, which excludes AOD but incorporates other features present in the Full model, slightly outperformed the AOD model by 0.01 in R^2 and within R^2 (Figure S16). This suggests that, at least in our setting, TROPOMI data can be a substitute for AOD in predicting $PM_{2.5}$ concentrations, which is perhaps appealing given their lower amount of missing data compared to AOD. Nevertheless, the combined use of both TROPOMI and AOD features provides the strongest predictive power (Figure S16).

Long-term spatiotemporal trends in predicted $PM_{2.5}$ concentrations

To better understand longer-term shifts in $PM_{2.5}$ concentrations, we calculate the changes in average $PM_{2.5}$ concentrations between six-year blocks, beginning in 2005-2010 (Figure 2A) and ending in either 2011-2016 (Figure 2B) or 2017-2022 (Figure 2C). We find that much of India experienced substantial increases in $PM_{2.5}$ concentrations between 2011-2016 compared to 2005-2010, except for regions such as Jammu and Kashmir, Punjab, and Rajasthan states. However, the pace of increase moderated in more recent years, and during 2017-2022, a higher percentage of locations across the country showed decreases in $PM_{2.5}$ concentrations (45 % of grid cells at a 10 km resolution) compared to 2011-2016 (16 % of grid cells), with notable decreases observed in Jammu and Kashmir, Punjab, Haryana, Delhi, and Rajasthan states and union territories.

To characterize trends in $PM_{2.5}$ concentrations, we quantify population-weighted annual average $PM_{2.5}$ concentrations for the country overall and five mega-cities from 2005 to 2022 (Figure 2D) by combining our 10km $PM_{2.5}$ estimates with gridded population data. Among the five mega-cities, the average New Delhi resident has consistently faced the highest population-weighted average of $PM_{2.5}$ concentrations, with 88.67 μg/m^3 in 2022, more than double India's annual national air quality guideline of 40 μg/m^3 (*41*) (Figure 2D). Similarly, residents in India overall, as well as those in Kolkata and Mumbai, have consistently experienced $PM_{2.5}$ levels exceeding the national annual threshold (Figure 2D). Notably, we estimate that residents in all mega-cities have experienced a moderate decline in $PM_{2.5}$ exposure since 2016-2018 (Figure 2D), as assessed by computing the 3-year rolling averages of population-weighted $PM_{2.5}$ concentrations (Figure 2E). Mumbai exhibited the most substantial decline of 10 %, followed by New Delhi with 8 % in 2020-2022 (Figure 2E).

We further examine whether the observed declining trend since 2016-2018 is attributable to meteorological variability, including increasing trends in precipitation and relative humidity (*42*, *43*) observed in 70 % and 90 % of 10 km grid cells, respectively, from 2005-2015 to 2016-2022 (Figure S17). Employing trend analysis (see Materials and Methods), we compare the observed average annual trend for 2005-2015 and 2016-2022 with the meteorology-corrected trend for the same periods. Our analysis revealed that the declining trend in $PM_{2.5}$ concentrations from 2016 to 2022 was influenced by meteorological variability in the southern regions, but not in the northern regions such as Delhi, Haryana, Rajasthan, Uttar Pradesh, and Bihar (Figure S18). This suggests that without meteorological influence, the southern regions would have experienced fewer decreases in $PM_{2.5}$ concentrations from 2016 to 2022. In contrast, we find little evidence that the increasing trend from 2005 to 2015 was driven by changing meteorology (Figure S18), suggesting that these increases could be attributable to increased anthropogenic activities. We then confirm these trends using emissions data obtained from the Emissions Database for Global Atmospheric Research (EDGAR) (*44*, *45*), focusing particularly on $PM_{2.5}$ and Black Carbon (BC) emissions. Notably, nationwide declines in BC emissions were observed in 2018 compared to 2016, and some locations experienced decreases in $PM_{2.5}$ emissions in 2018 (Figure S19). When emissions data beyond 2018 becomes available, further analysis can confirm whether the declining trend in $PM_{2.5}$ concentrations align with $PM_{2.5}$ and BC emissions in more recent years.

As declines in $PM_{2.5}$ since 2016 are not attributed to favorable meteorology, we examine whether India's air quality control policies, particularly the National Clean Air Programme (NCAP), might have contributed to recent reductions in ambient $PM_{2.5}$ concentrations. Acknowledging the need for improved air quality to reduce health and societal burdens in the country, the government of India has recently proposed and implemented a number of air quality control measures, such as NCAP, the Bharat Stage-VI (BS-VI) emission standards for vehicles that mandated vehicles to adhere to PM emission limits as strict as European standards, which went into effect in Delhi in 2018 and other parts of India in 2020 (*46*), and the closure of multiple coal-fired power plants located near the Delhi National Capital Region (NCR) (*47*). However, the specific contribution of each policy to improving nationwide and regional air quality remains uncertain.

NCAP was initiated in 2019 with the goal of reducing key air pollutants, including $PM_{2.5}$, by 20 to 30% by 2024, using the pollution levels observed in 2017 as a baseline (*7*). Focusing on 131 non-attainment cities across 28 states and union territories, selected based on air quality data from 2015 to 2019 (*7*), one of the primary objectives of NCAP is to prompt each non-attainment city to prepare and implement a clean air action plan that details sector-specific interventions to improve air quality with predetermined timelines and an agency responsible for execution of each intervention (*7*, *11*). Under the NCAP, 102 out of the 131 non-attainment cities submitted comprehensive city action plans, which were approved by the CPCB in July 2020 (*11*).

We use a difference-in-differences approach to assess whether the implementation of the NCAP has affected changes in ambient $PM_{2.5}$ concentrations to date. Our approach compares within-subdistrict changes in $PM_{2.5}$ over time, in targeted and non-targeted areas, before and after initiation of NCAP. Our analysis is constrained to the subdistrict level, rather than the city level, due to the limited availability of reliable city-level shapefiles in India. We denote "treated" subdistricts as the 102 non-attainment cities whose city clean action plans were approved in 2020, and select a set of corresponding control subdistricts that were not targeted by NCAP using a propensity score method that matches pre-treatment trends in air pollution and covariates between later-treated and never-treated subdistricts (see Materials and Methods). To account for spillover effects, we exclude subdistricts adjacent to treatment subdistricts and any others within a 50 km buffer. Consequently, 88 treatment subdistricts and 74 control subdistricts are included (Figure S20), and the effect of NCAP is estimated by comparing whether trends in air pollution diverged between treated and control units after 2020. Our analysis reveals that there is no evidence that NCAP contributed to reducing $PM_{2.5}$ concentrations both in 2021 and 2022 (Figure S21) in targeted cities.

The observed decreases in $PM_{2.5}$ concentrations, especially in the mega-cities in 2020, are instead more consistent with previous studies examining the impact of the COVID-19 pandemic on air quality in India (*48–52*), which highlighted a significant decrease (43%) in $PM_{2.5}$ in 2020 compared to 2017-2019 in urban areas, after controlling for meteorological variability (*48*). Other various air quality control policies in India, including the implementation of BS-VI emission standards and the closure of power plants near Delhi, may have contributed to the nationwide or regional $PM_{2.5}$ declines. Our $PM_{2.5}$ estimates could be used to evaluate the impact of these programs in future work.

Population exposure to $PM_{2.5}$ concentrations

To understand the population exposure to daily high levels of $PM_{2.5}$ concentrations, we calculate the average number of days that each grid cell exceeded the WHO guideline of 15 $\mu g/m^3$, the national guideline of 60 $\mu g/m^3$, and the extreme concentration of 100 $\mu g/m^3$ between 2018 and 2022. Notably, much of India experienced over 300 days above the WHO daily threshold, except for the northeastern region (Figure 3A). Delhi, Rajasthan, Uttar Pradesh, and Bihar encountered days exceeding the national guideline of 60 $\mu g/m^3$ for at least 250 days (Figure 3A). Moreover, certain locations in Delhi, Uttar Pradesh, and Bihar observed extreme days with $PM_{2.5}$ concentrations exceeding 100 $\mu g/m^3$ for 100 to 150 days (Figure 3A).

We also assess the proportion of the overall population exposed to elevated annual concentrations of $PM_{2.5}$ over our study period. Notably, the entire population in India has consistently faced exposure above the WHO annual threshold of 5 $\mu g/m^3$ over the 17 years (Figure 3B). Although there was a decrease in 2020, approximately 60% of the population consistently experienced exposure exceeding the national annual guideline of 40 $\mu g/m^3$, and 10% experienced extreme levels of $PM_{2.5}$, with an annual average of 80 μg/m^3 (Figure 3B). Further analysis of the spatial distribution of these exposed populations revealed that 63% of the locations exceeded the national guideline between 2018 and 2022 (Figure 3C). Areas with annual average $PM_{2.5}$ concentrations exceeding 80 μg/m^3 were predominantly observed around Delhi and in Bihar state (Figure 3C).

Inequalities in $PM_{2.5}$ exposure

Identifying disparities in $PM_{2.5}$ exposure by socio-economic status is essential to understanding pollution burdens and developing policy measures to alleviate them. To understand how pollution concentrations vary with socioeconomic status in India, we combine recent high-resolution estimates of local-level asset wealth (*54*), a common proxy for socioeconomic status, with spatial and temporal variation in our $PM_{2.5}$ predictions at a 10 km resolution.

Utilizing 5-year average $PM_{2.5}$ concentrations from 2015 to 2019 (see Materials and Methods), we find that the wealthiest quintile of the population is slightly less likely to experience concentrations above the national annual guideline of 40 μg/m^3 as compared to other quintiles of the wealth distribution (Figure 4A) – although substantial majorities in all quintiles are exposed to levels above this guideline. However, areas in the top two wealth quintiles are substantially more likely to live in areas with extreme $PM_{2.5}$ concentrations above 80 μg/m^3 annually (23.0 % and 21.0 %, respectively) (Figure 4B), consistent with a previous study revealing that wealthy populations live in polluted urban centers in low- and middle-income countries (*3*). Due to these extreme exposures, an average person at the 90th percentile of wealth in India has consistently faced higher $PM_{2.5}$ exposure than the average Indian or someone at the 10th percentile of wealth from 2005 to 2022, holding wealth constant across years (Figure 4C). Notably, since 2016, an average wealthy individual has also experienced faster declines in $PM_{2.5}$ concentrations than an average poor individual, particularly evident since the start of the COVID-19 pandemic, yet notably apparent as early as 2017-2019. (Figure 4C, 4D, S23). This has shrunk the wealth gap in average $PM_{2.5}$ over time. These $PM_{2.5}$ reductions disproportionately experienced by wealthier individuals highlights the urgent need of air quality mitigation policies that effectively target both the poor and the rich.

Assessing the optimal placement of air quality monitors ensuring equality

The current CAAQMS network is sparser in poorer communities, limiting understanding of disproportionate $PM_{2.5}$ exposure. While our predictions enable investigation of nationwide trends and exposure across wealth groups, ground monitor data would enhance precision of such monitoring and ground monitor data will likely remain the basis for official evaluation of air quality trends and policy attainment. The government of India has committed to expanding the CAAQMS up to 1,000 monitors under NCAP(*11*) to aid in more comprehensive air pollution monitoring. However, it is uncertain whether placement decisions account for the ability to accurately monitor pollution concentrations across the socioeconomic spectrum.

We use compressed sensing methods (*37*, *55*) to propose strategic placement of additional 565 CAAQMS monitors, or the remainder of the 1,000 total monitors proposed to be installed under NCAP, using data from our AOD model to inform monitor placement (see Materials and Methods). Our approach identifies baseline national-scale long-term variability of $PM_{2.5}$ concentrations, and then chooses locations of additional monitors that would optimally capture local and short-term anomaly spikes in $PM_{2.5}$ exceeding this baseline across the country. When placing monitors, we prioritize low-wealth locations to ensure that sudden spikes occurring in poorer communities are also captured. The identified placement of monitors (Figure 5A) highlights the need for an additional dense network in northern India, particularly in Rajasthan, Delhi, Haryana, Uttar Pradesh, Bihar, and Assam states and union territories, as well as in the southeastern region, including West Bengal and Telangana states. The proposed additional network would help promote equality in nationwide exposure assessment while also enabling the network to maximally capture spatial and temporal variation in surface $PM_{2.5}$ concentrations.

Examining applicability of our model to other low- and middle-income settings

Other low- and middle-income countries also face challenges in understanding overall levels and trends in population exposure to $PM_{2.5}$ as well as inequalities in these exposures, due to limited ground-monitoring data. Our method could provide resource-efficient alternative to establishing extensive monitoring network by generating predictions for non-monitored locations, but it relies on having at least some amount of ground monitoring data to train and validate predictions. To understand how the performance of our machine learning approach changes as the ground network becomes sparser, we vary the number of monitors our model is allowed to see in training and quantify the relationship between the number of monitors in training and model performance. To estimate uncertainty in performance, we repeat this experiment a thousand times, resampling a fixed number of stations for training each time and re-estimating model performance on a disjoint set of sampled test stations (for more details, see Materials and Methods).

We observed an nonlinear increase in model performance, as evaluated on held-out test monitors, ranging from an R^2 value of 0.50 to 0.33 with 25 monitors, and reaching R^2 values of 0.68 and 0.54 with 300 monitors (Figure 5B). When evaluated at the monthly level using the same sets of daily predictions derived from this experiment, we achieved R^2 and within R^2 values comparable to those of the existing benchmark publicly-available monthly $PM_{2.5}$ dataset(*14*) (Figure S7) while training only on 25 and 50 monitors, respectively (Figure 5C). These results indicate that investment in a moderate number of reference-grade air quality monitors, when combined with information from satellites, can enable training of machine-learning-based model that can predict $PM_{2.5}$ concentrations with performance that exceeds benchmark datasets commonly used for health impact analysis in low- and middle-income countries. While variations in $PM_{2.5}$ concentrations and country sizes differ, these findings offer valuable insights for other countries designing their monitoring network and implementing our machine learning method to understand nationwide trends and exposure to $PM_{2.5}$ across different populations.

DISCUSSION

Here, we generate daily $PM_{2.5}$ predictions at a spatial resolution of 10 km across India from 2005 to 2023. These daily estimates perform well over the range of observed monitor $PM_{2.5}$ measurements, and very accurately capture temporal variations in $PM_{2.5}$ concentrations, including daily peaks, within mega-cities in India. We find a declining trend in average $PM_{2.5}$ concentrations since 2016-2018, particularly in northern India, and confirm that these reductions are not attributable to meteorological variability nor to NCAP, a recently-begun nationwide air quality improvement program; smaller declines in southern India are driven in part by favorable trends in meteorology. Our analysis also provides a comprehensive characterization of the spatial distribution of populations exposed to elevated levels of daily and annual $PM_{2.5}$, revealing that wealthier people are more likely to live in areas with extreme $PM_{2.5}$ concentrations but that they have also experienced faster reductions in exposure in recent years. We propose the strategic placement of additional CAAQMS monitors to more effectively capture high $PM_{2.5}$ episodes occurring in both poorer and wealthier locations, and we study the applicability of our approach in settings where existing or proposed monitoring networks could be even sparser than in our Indian study context, finding that only a relatively small number of monitors are needed to train a relatively accurate prediction model.

In comparison to many existing efforts to estimate $PM_{2.5}$ concentrations using machine learning (*27*, *28*), we incorporate data from multiple recent satellite sensors to estimate pollution concentrations across the country. Additionally, we spatially validate predictions against time series of held-out monitor observations, which stands in contrast to the random CV used in many previous machine learning-based efforts (*24*, *25*, *56*, *57*). Finally, our work complements recent machine learning-based studies to estimate $PM_{2.5}$ concentrations by providing insights into the predictive power of TROPOMI features in contrast to AOD.

Our $PM_{2.5}$ predictions could likely be further improved through improvements in both the monitor-based ground truth data and in the remotely-sensed input features. Our method relies on ground $PM_{2.5}$ observations acquired from CAAQMS monitors for training; however, the management of these monitors and quality of the collected data has not been verified by a third-party institution (*5*). For instance, in the UK, all regulatory air quality data collected as part of the Automatic Urban and Rural Network is validated by an independent agency (*5*). Using the quality-assured ground measurements could help improve our predictions by reducing noise in both model training and validation. Additionally, future model development could benefit from additional monitor data, including PurpleAir monitors and CPCB's manual monitoring stations. Calibration is imperative for these data as they are not considered as reference grade or regularly calibrated. Calibration of PurpleAir measurements to estimate $PM_{2.5}$ concentrations has been widely explored by previous studies (*58–62*). A recent study (*63*) highlights the significance of seasonally-optimized calibration for PurpleAir sensors in enhancing prediction performance, especially in India. Calibration of manual monitor measurements is also crucial since $PM_{2.5}$ samples are collected for 8 hours twice a week, providing only a snapshot of actual concentrations (*5*). Moreover, the remotely-sensed input features utilized in our model, particularly TROPOMI data, do not directly represent air pollution concentrations at the ground level. A recent study (*64*) revealed a mean relative and absolute bias of approximately 10 % between TROPOMI NO_2 products and ground-based observations, highlighting a tendency for frequent underestimation of elevated NO_2 levels on the ground (*64*). The robust predictive power of TROPOMI features indicates that the calibration of these data could lead to improved performance of machine learning-based estimations for $PM_{2.5}$ concentrations, although our machine-learning-based approach is implicitly calibrating these satellite observations to ground data already. Finally, uncertainty quantification from machine learning models is currently an active area of research. Subsequent enhancements to $PM_{2.5}$ estimates may involve more granular quantification of uncertainty.

Another limitation of our study is that we relied on cross-sectional wealth estimates for investigating temporal changes in wealth disparities in $PM_{2.5}$ exposure. The wealth data we used for India were derived from machine learning models trained on ground data from 2015 and 2019, and thus might not capture shifts in the wealth distribution in other years. While these wealth estimates represent the most comprehensive and up-to-date local-level estimates of income or wealth in India that we are aware of (*3*, *54*), future improvements to these data could further improve our understanding of spatial distribution of and temporal changes in income disparities in $PM_{2.5}$ exposure across the country.

Our publicly available $PM_{2.5}$ predictions serve as a platform for evaluating specific policies or interventions aimed at improving air quality. We utilized our daily $PM_{2.5}$ estimates in the initial evaluation of India's NCAP, finding a limited impact of the program to date in targeted cities. This null result could be because city-level clean air action plans did not yet have time to take effect, or because they are not effective, and our $PM_{2.5}$ data – which can be updated in future years – offer a platform for understanding which explanation is more likely true. They also offer the critical opportunity to evaluate other air quality control measures being rolled out across the country, as well as an opportunity to identify the contribution to local $PM_{2.5}$ concentrations of emissions from specific sources such as brick kilns that exhibit distinct spatial and temporal patterns. Finally, our data could also be used to better assess the health burden on air pollution in the country – a task often accomplished using existing monthly $PM_{2.5}$ datasets that are more temporally coarse and less accurate than the data we produce here.

MATERIALS AND METHODS

Model inputs

We collect daily $PM_{2.5}$ observations from January 1, 2013, to September 30, 2023, from 435 CAAQMS monitors with accessible geo-coordinate information, serving as ground truth for our machine learning model. We construct two main machine learning models to predict $PM_{2.5}$ concentrations: the AOD model and the Full model. The input features of the AOD model include MODIS AOD, meteorology, land cover, and elevation collected from the Google Earth Engine (GEE) platform, along with atmospheric reanalysis data retrieved from NASA's Earthdata portal. In addition to these features, the Full model incorporates Sentinel-5P mission's TROPOMI for NO_2 and CO, launched on October 13, 2017, by the European Space Agency. The AOD model is trained on ground-measured $PM_{2.5}$ from January 1, 2013, to September 30, 2023 and used to generate daily $PM_{2.5}$ predictions starting from January 1, 2005, which corresponds to the earliest available input feature for the model. Conversely, the Full model is trained from July 10, 2018, to September 30, 2023 due to the limited availability of TROPOMI features, and used to produce predictions for the corresponding period. Both $PM_{2.5}$ measurements and input features are merged to a consistent 10 km grid for model training and validation. The grid is constructed to cover country borders of the Republic of India as per survey of India records.

From the collected $PM_{2.5}$ observations, we exclude values of 999.99 μg/m^3, the upper detection limit of CCAQM monitors, as it does not accurately represent the actual concentration on the ground (*65*). Additionally, we filter out $PM_{2.5}$ measurements if the difference between the rolling average of the preceding 5 days and the $PM_{2.5}$ concentration on the current day is less than 0.05 to ensure that air quality monitors exhibit valid variations in daily concentration changes (i.e. we remove observations when they were at an unrealistic constant level for over five days). As a result, 4,213 observations (1.2%) were removed. Subsequently, for each 10 km grid, we exclude extreme outliers identified by an interquartile range (IQR) that fall below 15 times the first quartile or exceed 15 times the third quartile, resulting in the removal of 24 observations. The use of a threshold of 15 times allows us to identify $PM_{2.5}$ measurements that significantly deviate from the IQR within each 10 km grid, and helps retain elevated observations that may reflect local variations, such as those caused by agricultural fires.

The complete list of input features for the AOD and Full models can be found in Table S1. TROPOMI NO_2 (tropospheric vertical column of NO_2) (*35*) and CO (vertically integrated CO column density) (*36*) are derived from the Sentinel-5P gridded level 3 product at a 1.11 km resolution. AOD is collected from the MODIS Multi-angle Implementation of Atmospheric Correction (MAIAC) Land gridded Level 2 product ((0.55'μm), produced daily at a 1 km resolution (*34*). Meteorological input features comprise the daily mean of temperature and dewpoint temperature at 2 meters, wind speed in the eastward and northward directions, total precipitation, net thermal radiation at the surface, and surface pressure. These input features are drawn from the daily aggregate of European Centre for Medium-Range Weather Forecasts (ECMWF) Reanalysis 5th Generation (ERA5) land hourly assets at an 11.13 km resolution (*66*). Additionally, the daily mean of wind degree and relative humidity per 10 km grid is calculated using wind speed in the eastward and northward directions, temperature, and dewpoint temperature. Furthermore, we incorporate MODIS land cover type data produced yearly at a 500-meter resolution (*67*). In addition to MODIS land cover data, low and high vegetation indices obtained from ECMWF ERA5 are included in the model. Elevation data is sourced from the Shuttle Radar Topography Mission (SRTM) at a resolution of approximately 30 meters (*68*).

To account for missing observations in TROPOMI features and AOD, atmospheric reanalysis data such as the Modern-Era Retrospective Analysis for Research and Applications, version 2 (MERRA-2) aerosol optical thickness (AOT at 550nm) (*69*) and CO (*70*), as well as Aura Ozone Monitoring Instrument (OMI) NO_2 (*71*), are included. Importantly, those missing data in TROPOMI features and AOD are imputed using machine learning methods before being incorporated into the main machine learning model, which predicts $PM_{2.5}$ concentrations. Furthermore, the missingness of TROPOMI NO_2, CO, and AOD is computed based on the amount of missing observations for each day, and this information is included as model input. Finally, month and day of the year, a dummy variable indicating a monsoon season, and centroids of each 10 km grid are incorporated as model input features. Weekly rolling averages of TROPOMI NO_2 and CO, AOD, MERRA-2 variables, and meteorological variables are also calculated and included in the model to capture the potential time dependency between input features and $PM_{2.5}$ observations to improve the model predictability.

Imputation of TROPOMI and AOD

For the Full model, 26.0% of TROPOMI NO_2, 18.7% of TROPOMI CO, and 49.0% of AOD had missing observations from July 10, 2018, to September 30, 2023 across the country (Figure S24). In the AOD model, 41.8% of AOD data was missing from January 1, 2013, to September 30, 2023 (Figure S25). These missing observations are predicted using light gradient-boosting machine (LightGBM) and XGBoost with input features, including MERRA-2 AOT and CO, OMI NO_2, meteorology, land cover, elevation, month and day of the year, a dummy variable indicating a monsoon season, centroids of each 10 km grid, and weekly rolling averages and annual averages of MERRA-2 variables, as well as meteorological variables (Table S2). We conduct pairwise correlation analysis for feature selection to ensure no variable is highly correlated ($R^2 > 0.9$) with each other, resulting in the removal of redundant features and increased efficiency in learning tasks (*72*).

Models are trained on TROPOMI NO_2, TROPOMI CO, and AOD observations for each machine learning task to predict and impute missing data using randomly-selected training data (2% for models predicting TROPOMI NO_2 and TROPOMI CO, and 3% for the model predicting AOD) based on 50 km grid cells, month of the year, and year. For model selection and hyperparameter tuning, we conduct 5-fold inner spatial CV using training data in one of the 10-fold outer spatial CV to prevent any final test data from leaking into training tasks during model selection and hyperparameter tuning. Both the inner and outer spatial CV are conducted based on 50 km grid to account for spatial auto-correction within the input features, especially MERRA-2 reanalysis data, which has the most coarse spatial resolution of approximately 50 km (0.5° latitude × 0.625° longitude). Splitting data into training and test sets based on the 50 km grid, rather than the more conventional method of random splitting by observation is a more demanding prediction task because a given monitor can contribute data to both training and test sets in case of random split. Using coarser spatial blocks, rather than 10 km grid, further increases the difficulty of such a task; however, spatial CV is a more realistic test of how well the model would perform in predicting time series of missing observations in a new location with no training data. We fit LightGBM and XGBoost for each model predicting TROPOMI NO_2, TROPOMI CO, and AOD while implementing GridSearchCV to search over the LightGBM and XGBoost hyperparameter ranges (Table S3) and identify the optimal combination of hyperparameters. As a result, LightGBM was used for predicting missing TROPOMI NO_2 and TROPOMI CO, and XGBoost was used for predicting missing AOD (Table S4). The final predictions derived from held-out test data in each of the 10 folds are compared with observations using the evaluation metrics, such as overall R^2, within R^2, and RMSE. The within R^2 is calculated by regressing observed TROPOMI NO_2, TROPOMI CO, and AOD on their respective predicted values while incorporating fixed effects for locations with observations, month of the year, and year.

For the Full model, the predictions of missing TROPOMI NO_2 explained 52%, predictions of missing TROPOMI CO explained 92%, and predictions of missing AOD explained 82% of out-of-sample variation (Table S5). For the AOD model, the predictions of AOD explained 82% of out-of-sample variation (Table S5). We then predicted TROPOMI NO_2, TROPOMI CO, and AOD values for all 10 km grid cells over India, and used these imputed variables as input features for the main machine learning model predicting $PM_{2.5}$ concentrations. Binary variables indicating whether each of TROPOMI NO_2, TOPOMI CO, and AOD is imputed (0 or 1) is also included. Finally, we create additional weighted variables by assigning weights to the imputed TROPOMI NO_2, TROPOMI CO, and AOD values based on their respective imputation performances (1.0 for actual observations, 0.5 for imputed TROPOMI NO_2, 0.9 for imputed TROPOMI CO, and 0.8 for imputed AOD). The weighted variables are incorporated into the main machine learning model.

Model tuning and validation

The Full model is trained and validated on 301,355 daily ground-measured $PM_{2.5}$ concentrations from July 10, 2018, to September 30, 2023. The AOD model is trained on 345,559 $PM_{2.5}$ observations from January 1, 2013, to September 30, 2023. Similar to our models for the imputation of TROPOMI features and AOD, we conduct pairwise correlation analysis for feature selection to ensure no variable is highly correlated ($R^2 > 0.9$) with each other. For model selection and hyperparameter tuning, we conduct 5-fold inner spatial CV using training data in one of the 10-fold outer spatial CV. Both the inner and outer spatial CV are constructed based on 50 km grid. When splitting data into training and test sets through inner and outer spatial CV, we ensure that each test fold includes a nearly equal number of 50 km grid cells from each of three environmental regions (Figure S5), identified based on k-means clustering using imputed TROPOMI NO_2 and CO, imputed AOD, MERRA-2 AOT and CO, and OMI NO_2. This helps balance environmental characteristics, such as urban versus rural, within training and test data in each fold. For the inner 5-fold CV, each 50 km block of 10 km grid cells goes into only one of the 5 test folds, and for the outer 10-fold CV, each 50 km block goes into only one of the 10 test folds. We fit LightGBM and XGBoost using the inner CV while implementing GridSearchCV to search over the hyperparameter ranges and identify the optimal combination of hyperparameters (Table S6). Based on the model performances using the inner CV, we selected XGBoost for both Full and AOD models (Table S7). We apply XGBoost to the outer 10-fold spatial CV, utilizing the RMSE as the objective function.

We measure model performance by comparing observed $PM_{2.5}$ with model predictions derived from held-out test data in each of the 10 folds. For the model evaluation, we calculate overall R^2, within R^2, and RMSE on the held-out test set for each of the 10 folds. Similar to the models for imputing missing observations in TROPOMI NO_2, TROPOMI CO, and AOD, the within R^2 is calculated by regressing observed $PM_{2.5}$ concentrations on predicted values while incorporating fixed effects for locations with observations, month of the year, and year.

Sensitivity analysis

As part of the sensitivity analysis, we aim to assess the robustness of the Full model by exposing it to a more spatially challenging task through the implementation of a 10-fold spatial CV with larger test blocks based on latitude (Figure S13). Additionally, we conduct another iteration of the Full model using a 10-fold random CV where data is randomly split into 10 folds without specific consideration for spatial distribution. This approach enables us to assess and confirm the potential underestimation of spatial prediction errors and the optimistic overall results associated with random k-fold CV, which does not account for spatial auto-correction within spatial data.

Predictive power of AOD and TROPOMI features

To evaluate and identify the predictive power of TROPOMI features, we construct another model, the TROPOMI model, which excludes AOD but incorporates other features present in the Full model. We compare the performance of the Full, AOD, and TROPOMI models by fitting XGBoost using the same training and test sets from July 10, 2018, to September 30, 2023. Evaluation metrics include the overall R^2, within R^2, and RMSE.

Assessing long-term spatiotemporal trends in predicted $PM_{2.5}$ concentrations

Utilizing the $PM_{2.5}$ predictions derived from the AOD model, We calculate the average $PM_{2.5}$ concentrations per 10 km grid between 2005 and 2010, and changes in average concentrations from 2005-2010 to 2011-2016 and to 2017-2022. Employing six-year windows helps control for meteorological variability between years and mitigates undue influence from extreme years, such as 2020 when India experienced a nationwide lockdown, similar to other countries (*49*). Additionally, population-weighted annual average $PM_{2.5}$ concentrations are computed for India as a whole and five mega-cities from 2005 to 2022, combining population counts (*73*) with annual average $PM_{2.5}$ concentrations per 10 km grid. To elucidate the long-term temporal trend in population-weighted averages, we also calculate the percentage changes in population-weighted annual average $PM_{2.5}$ concentrations for each 3-year window from 2006-2008 to 2020-2022 relative to the 3-year average from 2005-2007.

Identifying the contribution of meteorological variability to long-term trends in predicted $PM_{2.5}$ concentrations

To identify the contribution of meteorological variability to the observed declining trend in $PM_{2.5}$ concentrations since 2016-2018, we model the $PM_{2.5}$ concentrations of each individual 10 km grid cell using an additive form of a trend component, a meteorology component, and time fixed effects (*42*). More specifically, we employ the following regression equation for each grid cell i:

$$y_{it} = \beta_i^{\mathrm{obs}} \times t + f_i(X_{it}) + \eta_{it} + \varepsilon_{it}$$

where y_{it} denotes the daily $PM_{2.5}$concentration at grid cell i on day t. t is the time index (e.g., $t = 1$ for 1 January 2005, $t = 2$ for 2 January 2005, and $t = 32$ for 1 February 2005). X_{it} denotes the local meteorology variables in grid cell i on day t, including temperature and dewpoint temperature at 2 meters, wind speed in the eastward and northward directions, total precipitation, and surface pressure. η_{it} is the month-of-year and day-of-month fixed effects to capture daily and monthly variability in pollutant concentrations that are not related to the meteorological variability (e.g., seasonal cycle in $PM_{2.5}$). ε_{it} is the normally distributed error term. β_i^{obs} represents the meteorology-corrected daily trend in $PM_{2.5}$ concentration for grid cell i estimated with the standard ordinary least-squares method. We apply the above regression equation to $PM_{2.5}$ daily predictions derived from the AOD model for 2005-2015 and 2016-2022, respectively, and obtain the meteorology-corrected annual trends of $PM_{2.5}$ concentrations for each grid cell for the corresponding periods by multiplying the estimated β_i^{obs} by 365 days.

In contrast, the observed annual trend is estimated by the following regression equation for each grid cell i:

$$y_{it} = \beta_i^{\text{obs}} \times t + \eta_{it} + \varepsilon_{it}$$

where y_{it} denotes the daily $PM_{2.5}$concentration at grid cell i on day t. t is the time index and η_{it} is the month-of-year and day-of-month fixed effects. ε_{it} is the normally distributed error term. Utilizing the β_i^{obs}, representing the daily trend in predicted $PM_{2.5}$ concentrations, annual trends for 2005-2015 and 2016-2022 are estimated.

Evaluation of NCAP

Our evaluation of NCAP is based on a matched difference-in-difference analysis, where we first identify a set of "control" urban areas that were not initially targeted by NCAP that look similar across a range of covariates to the "treated" cities that were targeted by the program, and then we compare trends in ambient $PM_{2.5}$ concentrations between treated and control areas, before and after program implementation. We implement our analysis at the subdistrict level due to the limited availability of city-level shapefiles in India. Specifically, we first identify the treatment subdistricts corresponding to the 102 non-attainment cities whose city clean action plans were approved in 2020. Next, we calculate the propensity score —the probability of becoming a city targeted by NCAP — based on population count, proportion of urban area, proportion of forest area, and total area per subdistrict using logistic regression. We apply this to non-treated subdistricts that are not adjacent to the treatment subdistricts and are located outside a 50 km radius from them to account for potential spillover effects of NCAP on neighboring subdistricts. Finally, we identify control subdistricts as those with propensity closest to those of the treatment subdistricts. Propensity score methods are commonly used to minimize selection bias in identifying control groups that share observed baseline characteristics with treatment groups as similar as possible (*74*). Consequently, our analysis includes 88 treatment subdistricts and 74 control subdistricts (Figure S20).

To establish the causal effect of NCAP, the trends in $PM_{2.5}$ concentrations in subdistricts that do not include NCAP's non-attainment cities must provide valid counterfactuals for the trends that we would have observed in the treatment subdistricts. We evaluate whether the parallel trends assumption may be reasonable in our case by plotting yearly average treatment effects on $PM_{2.5}$ concentrations prior to 2020, confirming that there was no systematic difference in treatment and control groups before city action plans were approved by the CPCB in 2020. More specifically, we employ the following regression equation to estimate the average treatment effects for each year from 2005 to 2022:

$$y_{it} = \sum_{j=t-15}^{t+2} \beta_j D_i * 1(year = j) + \alpha_i + \gamma_t + \theta x_{it} + \varepsilon_{it}$$

where y_{it} denotes the daily $PM_{2.5}$ concentration at subdistrict i on day t, and the β_j coefficients estimate the difference between treated and control subdistricts in the 15 years prior to treatment ($t = 0$, which is 2020 in our data, the year in which city clean action plans were approved by the CPCB), and the two observed years following treatment (2021 and 2022). The estimate in $t = 0$ is omitted to avoid collinearity, and so the β_j coefficients are interpreted as the difference between treated and control concentrations relative to the reference year of 2020. α_i represents a vector of subdistrict fixed effects, and γ_t vectors of month-of-year and year fixed effects. θx_{it} denotes a vector of additional time-varying controls at the subdistrict level, including temperature and dewpoint temperature at 2 meters, wind speed in the eastward and northward directions, total precipitation, and surface pressure. ε_{it} is the error term. Because our chosen treated units all adopted city clean action plans in the same year, our treatment is not staggered across time and thus our analysis avoids the inference issues that accompany difference-in-difference designs with staggered adoption that have been highlighted in recent literature.

Investigating population exposure to $PM_{2.5}$ concentrations

To identify locations with elevated levels of daily $PM_{2.5}$ concentrations, we employ predictions from the AOD model to calculate the average number of days each 10 km grid cell exceeding the WHO daily guideline of 15 μg/m^3, national daily guideline of 60 μg/m^3, and extreme value of 100 μg/m^3 for 2018-2022.

Furthermore, we examine proportional changes in populations exposed to high levels of $PM_{2.5}$ annual average concentrations from 2005 to 2022. For this analysis, we firstly calculate annual average $PM_{2.5}$ concentrations per 10 km grid. Subsequently, we identify the 10 km grids above the thresholds of the WHO annual guideline (5 μg/m^3), national annual guideline (40 μg/m^3), and extreme annual concentration (80 μg/m^3). We then aggregate the population counts residing in those grid cells exceeding each threshold to calculate the percentage of whole population.

Examining inequalities in $PM_{2.5}$ exposure

We combine estimates of relative wealth (Relative Wealth Indices (RWIs)) at a 2.4 km resolution (*54*) with our $PM_{2.5}$ predictions derived from the AOD model by averaging the wealth estimates for each 10 km grid. RWIs were generated using machine learning algorithms that utilized satellite data, mobile phone data, and data from Facebook users (*54*). For India, their machine learning algorithms were trained on ground measurements of wealth collected by DHS surveys in 2015 and 2019 (*54*). The gridded wealth data provide estimates for each grid cell of how wealthy that grid cell is relative to others in the same country as well as an estimated error for that estimate (*3*). We further combine population counts (*73*) for each grid, along with RWIs and daily $PM_{2.5}$ predictions from January 2005 to December 2022.

To understand the proportion of population exposed to elevated levels of $PM_{2.5}$ concentrations across wealth groups, we aggregate the population counts for 10 km grid cells whose average $PM_{2.5}$ concentrations for 2018-2022 are exceeding the national guideline of 40 μg/m^3 and extreme threshold of 80 μg/m^3 annually, respectively. We then calculate the percentage of population for each of the five wealth categories (Poorest, Poorer, Middle, Richer, and Richest), which are created based on quartiles of RWIs within the country. Additionally, to understand the temporal changes in wealth disparities in $PM_{2.5}$ exposure from 2005 to 2022, population-weighted annual average $PM_{2.5}$ concentrations are computed for all the wealth levels across the country, grid cells at 90th percentile of RWIs, and grid cells at 10th percentile of RWIs. To elucidate the long-term temporal trend in population-weighted averages, we also calculate the percentage changes in population-weighted annual average $PM_{2.5}$ concentrations for each 3-year window from 2006-2008 to 2020-2022 relative to the 3-year average from 2005-2007.

Assessing the optimal placement of air quality monitors ensuring equality

To calculate where additional ground monitors could be placed to optimally enhance the ability of the entire ground-monitoring network to capture spatial and temporal variation in ambient $PM_{2.5}$ concentrations, we use multi-resolution dynamic mode decomposition (mrDMD), which recursively decomposes a data set into low-rank spatial modes and their temporal Fourier dynamics. mrDMD has been shown to capture $PM_{2.5}$ concentrations spatially and temporally on short (daily) and long-term (years to decade) timescales, and to incorporate information from transient phenomena, such as wildfires and temperature inversions, that would otherwise be discarded or averaged out using similar data reduction techniques (*37*). The algorithm can thus capture a finer level of spatial and temporal variability in a data set that would otherwise be averaged out using traditional mean or maximum $PM_{2.5}$ metrics. mrDMD is a dimensionality reduction algorithm, similar to Principal Components Analysis (PCA), but mrDMD is more precise in capturing spatio-temporal variability than methods based on singular value decomposition such as PCA.

Here, we present an extension to the mrDMD framework that considers cost-constraining functions to optimize sensor placement based on wealth estimates. The mrDMD algorithm is based on a column-pivoted QR algorithm, where the pivot column is modified to balance (a) the decrease in accuracy of capturing the largest air pollution modal signals with (b) the increase in capturing pollution exposure in grid cells with low RWI values, representing poorer communities. The cost function used here is a step function that penalizes placing sensors too far from poorer locations. For the cost function vector, all data is a binary of 0 or 1, with 0 representing wealthy locations and 1 representing poor locations. More details of the method can be found in (*55*).

We apply all mrDMD methods to the $PM_{2.5}$ estimates derived from the AOD model from January 1, 2005, to September 30, 2023. The resulting sensor network adds additional monitors to the existing ground network in order to better constrain variation in surface pollution, and we select a number of additional monitors such that the entire monitoring network would have 1,000 ground monitors, an NCAP's target.

Examining applicability of our model to other low- and middle-income settings

To investigate the association between the quantity of ground truth data, represented by the number of 10 km grid cells with measured $PM_{2.5}$ observations, and the predictive performance of our machine learning model for $PM_{2.5}$ concentrations, we conduct an experiment involving multiple machine learning models trained with incremental training data. First, 21 out of 321 grid cells with $PM_{2.5}$ observations across the country are randomly selected and held out until the final evaluation of predictions. Second, from the remaining 300 grid cells, we randomly select grid cells in increments of 25, starting from 25 and up to 300 without replacement, respectively serving as training data for our Full model. This process result in the creation of 11 Full models with training data of different sizes. Each training dataset is then split into training and validation sets based on 50 km grid cells, creating a 10-fold spatial CV. For each model, XGBoost is applied with hyperparameter tuning, where the parameters include learning_rate (set to 0.01), lambda (1 or 10), max_depth (fixed at 10), and n_estimators (1,000 or 1,500), while keeping the remaining hyperparameters at their default values. The tuning process is performed using a 10-fold spatial CV. Finally, XGBoost with the best hyperparameters is applied to predict $PM_{2.5}$ concentrations for the initially randomly-selected 21 grid cells, and the final predictions are compared and evaluated with the test data. This entire process, from the random sampling without replacement of the 21 grid cells for the test dataset to making final predictions using the best hyperparameters for the 11 Full models, is repeated 1,000 times to obtain the best possible unbiased estimates of prediction performances. The mean within R^2 is calculated out of 1,000 samples for each of the 11 Full models.

Acknowledgments

We thank Stephen Luby, Eran Bendavid, Jessica Li, Chris Callahan, Sam Heft-Neal, Iván Higuera Mendieta, other members of Stanford ECHOLab, and seminar participants at IIT-Bombay for helpful comments. We also thank Sunil Dahiya from the Centre for Research on Energy and Clean Air for providing insights into India's air quality control policies. Some of the computing for this project was performed on the Stanford Sherlock cluster, and we would like to thank Stanford University and the Stanford Research Computing Center for providing computational resources and support that contributed to these research results. AK, KS, and EC acknowledge the support from the Horn Family Fellowship in Stanford's Emmett Interdisciplinary Program in Environment and Resources Fund. MQ acknowledges the support from the planetary health fellowship at Stanford's Center for Innovation in Global Health.

Author contributions

A.K., M.K., M.Q., and M.B. designed research; A.K. performed research; A.K., and M.K. analyzed data; and A.K., M.K., M.Q., K.S., E.C., and M.B. wrote the paper.

Competing interests

The authors declare no conflict of interest.

Data and materials availability

Our daily $PM_{2.5}$ datasets derived from the Full and AOD models have been deposited in Zenodo (`https://doi.org/10.5281/zenodo.10807119`) and are publicly available. Code and source data needed to replicate the results have been deposited in GitHub (`https://github.com/ayako-kawano/pm_prediction`).

References

1. R. Burnett *et al.*, Global estimates of mortality associated with long-term exposure to outdoor fine particulate matter. *Proceedings of the National Academy of Sciences* **115**, 9592–9597 (2018).

2. A Hajat, C Hsia, M. O'Neill, *Socioeconomic disparities and air pollution exposure: a global review. Curr Environ Health Rep 2 (4): 440–450, PMID: 26381684*, 2015.

3. A. P. Behrer, S. Heft-Neal, Higher air pollution in wealthy districts of most low-and middle-income countries. *Nature Sustainability*, 1–10 (2024).

4. J. Liu *et al.*, Disparities in air pollution exposure in the United States by race/ethnicity and income, 1990–2010. *Environmental health perspectives* **129**, 127005 (2021).

5. P. Pant *et al.*, Monitoring particulate matter in India: recent trends and future outlook. *Air Quality, Atmosphere & Health* **12**, 45–58 (2019).

6. A. Roychowdhury, A. Somvanshi, Breathing Space: How to track and report air pollution under the National Clean Air Programme. *Center for Science and Environment. Retrieved from https://www. cseindia. org/content/downloadreports/9923* (2020).

7. S. Guttikunda, N. Ka, T. Ganguly, P. Jawahar, Plugging the ambient air monitoring gaps in India's national clean air programme (NCAP) airsheds. *Atmospheric Environment* **301**, 119712 (2023).

8. S. Gulia, I. Khanna, K. Shukla, M. Khare, Ambient air pollutant monitoring and analysis protocol for low and middle income countries: An element of comprehensive urban air quality management framework. *Atmospheric Environment* **222**, 117120 (2020).

9. E. E. Agency, *European Air Quality Index* (`https://airindex.eea.europa.eu/Map/AQI/Viewer/#`), (accessed: 01.26.2024).

10. G. Geng *et al.*, Tracking air pollution in China: near real-time PM2. 5 retrievals from multi-source data fusion. *Environmental Science & Technology* **55**, 12106–12115 (2021).

11. T. Ganguly, K. L. Selvaraj, S. K. Guttikunda, National Clean Air Programme (NCAP) for Indian cities: Review and outlook of clean air action plans. *Atmospheric Environment: X* **8**, 100096 (2020).

12. P. N. deSouza *et al.*, An environmental justice analysis of air pollution in India. *Scientific reports* **13**, 16690 (2023).

13. J. Chakraborty, P. Basu, Air quality and environmental injustice in India: Connecting particulate pollution to social disadvantages. *International Journal of Environmental Research and Public Health* **18**, 304 (2021).

14. A. Van Donkelaar *et al.*, Monthly global estimates of fine particulate matter and their uncertainty. *Environmental Science & Technology* **55**, 15287–15300 (2021).

15. Q. Di *et al.*, An ensemble-based model of PM2. 5 concentration across the contiguous United States with high spatiotemporal resolution. *Environment international* **130**, 104909 (2019).

16. R. Rajak, A. Chattopadhyay, Short and long term exposure to ambient air pollution and impact on health in India: a systematic review. *International journal of environmental health research* **30**, 593–617 (2020).

17. M. L. Bell, A. Zanobetti, F. Dominici, Evidence on vulnerability and susceptibility to health risks associated with short-term exposure to particulate matter: a systematic review and meta-analysis. *Am J Epidemiol* **178**, 865–876 (2013).

18. Y. Wang, M. N. Eliot, G. A. Wellenius, Short-term changes in ambient particulate matter and risk of stroke: a systematic review and meta-analysis. *J Am Heart Assoc* **3** (2014).

19. H. Luo, Q. Zhang, Y. Niu, H. Kan, R. Chen, Fine particulate matter and cardiorespiratory health in China: A systematic review and meta-analysis of epidemiological studies. *J Environ Sci (China)* **123**, 306–316 (2023).

20. M. Kowalska, K. Kocot, Short-term exposure to ambient fine particulate matter (PM2,5 and PM10) and the risk of heart rhythm abnormalities and stroke. *Postepy Hig Med Dosw (Online)* **70**, 1017–1025 (2016).

21. R. Liang *et al.*, Effect of exposure to PM2.5 on blood pressure: a systematic review and meta-analysis. *J Hypertens* **32**, 2130–2140 (2014).

22. M. H. Li *et al.*, Short-term Exposure to Ambient Fine Particulate Matter Increases Hospitalizations and Mortality in COPD: A Systematic Review and Meta-analysis. *Chest* **149**, 447–458 (2016).

23. J. Fan, S. Li, C. Fan, Z. Bai, K. Yang, The impact of PM2.5 on asthma emergency department visits: a systematic review and meta-analysis. *Environ Sci Pollut Res Int* **23**, 843–850 (2016).

24. V. Katoch *et al.*, Addressing Biases in Ambient PM2. 5 Exposure and Associated Health Burden Estimates by Filling Satellite AOD Retrieval Gaps over India. *Environmental Science & Technology* (2023).

25. S. Dey *et al.*, A satellite-based high-resolution (1-km) ambient PM2. 5 database for India over two decades (2000–2019): applications for air quality management. *Remote Sensing* **12**, 3872 (2020).

26. S. Mandal *et al.*, Nationwide estimation of daily ambient PM2. 5 from 2008 to 2020 at 1sq. km. in India using an ensemble approach. *PNAS Nexus*, pgae088 (2024).

27. Z. Ma *et al.*, A review of statistical methods used for developing large-scale and long-term PM2. 5 models from satellite data. *Remote Sensing of Environment* **269**, 112827 (2022).

28. Y. Rybarczyk, R. Zalakeviciute, Machine learning approaches for outdoor air quality modelling: A systematic review. *Applied Sciences* **8**, 2570 (2018).

29. R. Koelemeijer, C. Homan, J Matthijsen, Comparison of spatial and temporal variations of aerosol optical thickness and particulate matter over Europe. *Atmospheric Environment* **40**, 5304–5315 (2006).

30. R. Son, D. Stratoulias, H. C. Kim, J.-H. Yoon, Estimation of surface Pm2. 5 concentrations from atmospheric gas species retrieved from tropomi using deep learning: impacts of fire on air pollution over Thailand. *Atmospheric Pollution Research* **14**, 101875 (2023).

31. M. L. Childs *et al.*, Daily local-level estimates of ambient wildfire smoke PM2. 5 for the contiguous US. *Environmental Science & Technology* **56**, 13607–13621 (2022).

32. L. Mamić, M. Gašparović, G. Kaplan, Developing PM2. 5 and PM10 prediction models on a national and regional scale using open-source remote sensing data. *Environmental Monitoring and Assessment* **195**, 644 (2023).

33. Y. Wang, Q. Yuan, T. Li, S. Tan, L. Zhang, Full-coverage spatiotemporal mapping of ambient PM2. 5 and PM10 over China from Sentinel-5P and assimilated datasets: Considering the precursors and chemical compositions. *Science of The Total Environment* **793**, 148535 (2021).

34. A. Lyapustin, Y. Wang, MODIS/Terra+Aqua Land Aerosol Optical Depth Daily L2G Global 1km SIN Grid V061. `https://doi.org/10.5067/MODIS/MCD19A2.061` (2022).

35. European Space Agency, "Copernicus Sentinel-5P (processed by ESA), 2021, TROPOMI Level 2 Nitrogen Dioxide total column products. Version 02", tech. rep.

36. European Space Agency, "Copernicus Sentinel-5P (processed by ESA), 2021, TROPOMI Level 2 Carbon Monoxide total column products. Version 02", tech. rep.

37. M. M. Kelp, S. Lin, J. N. Kutz, L. J. Mickley, A new approach for determining optimal placement of PM2. 5 air quality sensors: case study for the contiguous United States. *Environmental Research Letters* **17**, 034034 (2022).

38. United Nations, Department of Economic and Social Affairs, Population Division, "World Population Prospects 2022: Data Sources", Technical Report UN DESA/POP/2022/DC/NO. 9.

39. R. Jat, B. R. Gurjar, D. Lowe, Regional pollution loading in winter months over India using high resolution WRF-Chem simulation. *Atmospheric Research* **249**, 105326 (2021).

40. M. S. Bhat, Q. S. Afeefa, K. P. Ashok, A. G. Bashir, Brick kiln emissions and its environmental impact: A Review. *Journal of Ecology and the Natural Environment* **6**, 1–11 (2014).

41. M. Kutlar Joss, M. Eeftens, E. Gintowt, R. Kappeler, N. Künzli, Time to harmonize national ambient air quality standards. *International Journal of Public Health* **62**, 453–462 (2017).

42. M. Qiu, C. Zigler, N. E. Selin, Statistical and machine learning methods for evaluating trends in air quality under changing meteorological conditions. *Atmospheric chemistry and physics* **22**, 10551–10566 (2022).

43. A. P. Tai, L. J. Mickley, D. J. Jacob, Correlations between fine particulate matter (PM2. 5) and meteorological variables in the United States: Implications for the sensitivity of PM2. 5 to climate change. *Atmospheric environment* **44**, 3976–3984 (2010).

44. J.-P. Jalkanen *et al.*, Extension of an assessment model of ship traffic exhaust emissions for particulate matter and carbon monoxide. *Atmospheric Chemistry and Physics* **12**, 2641–2659 (2012).

45. L. Johansson, J.-P. Jalkanen, J. Kukkonen, Global assessment of shipping emissions in 2015 on a high spatial and temporal resolution. *Atmospheric Environment* **167**, 403–415 (2017).

46. R. Lathia, S. Dadhaniya, Policy norms and proposed ways to achieve goals of Indian vehicle emission program. *Journal of Cleaner Production* **208**, 1339–1346 (2019).

47. A. K. Choubey, Lok Sabha Unstarred Question No. 2059. (July 2021).

48. S. Sharma, M. Zhang, J. Gao, H. Zhang, S. H. Kota, *et al.*, Effect of restricted emissions during COVID-19 on air quality in India. *Science of the total environment* **728**, 138878 (2020).

49. M. Marwah, P. K. Agrawala, COVID-19 lockdown and environmental pollution: an Indian multi-state investigation. *Environmental Monitoring and Assessment* **194**, 49 (2022).

50. S. K. Sahu *et al.*, Establishing a link between fine particulate matter (PM2. 5) zones and COVID-19 over India based on anthropogenic emission sources and air quality data. *Urban Climate* **38**, 100883 (2021).

51. R. L. Verma, J. S. Kamyotra, *et al.*, Impacts of COVID-19 on air quality in India. *Aerosol and Air Quality Research* **21**, 200482 (2021).

52. S. Gulia *et al.*, COVID 19 Lockdown-air quality reflections in Indian cities. *Aerosol and Air Quality Research* **21**, 200308 (2021).

53. W. H. Organization *et al.*, *WHO global air quality guidelines: particulate matter (PM2. 5 and PM10), ozone, nitrogen dioxide, sulfur dioxide and carbon monoxide* (World Health Organization, 2021).

54. G. Chi, H. Fang, S. Chatterjee, J. E. Blumenstock, Microestimates of wealth for all low-and middle-income countries. *Proceedings of the National Academy of Sciences* **119**, e2113658119 (2022).

55. M. M. Kelp *et al.*, Data-driven placement of PM2. 5 air quality sensors in the United States: An approach to target urban environmental injustice. (2023).

56. A. Brenning, presented at the 2012 IEEE international geoscience and remote sensing symposium, pp. 5372–5375.

57. P. Tziachris *et al.*, Spatial or Random Cross-Validation? The Effect of Resampling Methods in Predicting Groundwater Salinity with Machine Learning in Mediterranean Region. *Water* **15**, 2278 (2023).

58. L. Wallace, J. Bi, W. R. Ott, J. Sarnat, Y. Liu, Calibration of low-cost PurpleAir outdoor monitors using an improved method of calculating PM2. 5. *Atmospheric Environment* **256**, 118432 (2021).

59. K. K. Barkjohn, B. Gantt, A. L. Clements, Development and application of a United States-wide correction for PM 2.5 data collected with the PurpleAir sensor. *Atmospheric Measurement Techniques* **14**, 4617–4637 (2021).

60. W. W. Delp, B. C. Singer, Wildfire smoke adjustment factors for low-cost and professional PM2. 5 monitors with optical sensors. *Sensors* **20**, 3683 (2020).

61. J. Bi, A. Wildani, H. H. Chang, Y. Liu, Incorporating low-cost sensor measurements into high-resolution PM2. 5 modeling at a large spatial scale. *Environmental Science & Technology* **54**, 2152–2162 (2020).

62. B. Feenstra *et al.*, Performance evaluation of twelve low-cost PM2. 5 sensors at an ambient air monitoring site. *Atmospheric Environment* **216**, 116946 (2019).

63. M. J. Campmier *et al.*, Seasonally optimized calibrations improve low-cost sensor performance: long-term field evaluation of PurpleAir sensors in urban and rural India. *Atmospheric Measurement Techniques* **16**, 4357–4374 (2023).

64. I. Ialongo, H. Virta, H. Eskes, J. Hovila, J. Douros, Comparison of TROPOMI/Sentinel-5 Precursor NO 2 observations with ground-based measurements in Helsinki. *Atmospheric measurement techniques* **13**, 205–218 (2020).

65. D. Sharma, D. Mauzerall, *et al.*, Analysis of air pollution data in India between 2015 and 2019. *Aerosol and Air Quality Research* **22**, 210204 (2022).

66. Copernicus Climate Change Service (C3S), *ERA5: Fifth generation of ECMWF atmospheric reanalyses of the global climate*, (2023-10-30) (`https://cds.climate.copernicus.eu/cdsapp#!/home`).

67. M. Friedl, D. Sulla-Menashe, *MODIS/Terra+Aqua Land Cover Type Yearly L3 Global 500m SIN Grid V061 [Data set]*, NASA EOSDIS Land Processes Distributed Active Archive Center, Accessed 2023-10-30 from `https://doi.org/10.5067/MODIS/MCD12Q1.061`, 2022.

68. T. Farr *et al.*, The Shuttle Radar Topography Mission. *Reviews of Geophysics* **45**, RG2004 (2007).

69. Global Modeling and Assimilation Office (GMAO), *MERRA-2 tavg1_2d_lnd_Nx: 2d,1-Hourly,Time-Averaged,Single-Level,Assimilation,Land Surface Diagnostics V5.12.4*, Greenbelt, MD, USA, Goddard Earth Sciences Data and Information Services Center (GES DISC), Accessed: [2023-10-30], `10.5067/RKPHT8KC1Y1T`, 2015.

70. Global Modeling and Assimilation Office (GMAO), *MERRA-2 inst3_3d_chm_Nv: 3d,3-Hourly,Instantaneous Level,Assimilation,Carbon Monoxide and Ozone Mixing Ratio V5.12.4*, Greenbelt, MD, USA, Goddard Earth Sciences Data and Information Services Center (GES DISC), Accessed: [2013-10-30], `10.5067/HO9OVZWF3KW2`, 2015.

71. N. A. Krotkov *et al.*, *OMI/Aura NO2 Cloud-Screened Total and Tropospheric Column L3 Global Gridded 0.25 degree x 0.25 degree V3*, NASA Goddard Space Flight Center, Goddard Earth Sciences Data and Information Services Center (GES DISC), Accessed: [2023-10-30], `10.5067/Aura/OMI/DATA3007`, 2019.

72. L. Yu, H. Liu, presented at the Proceedings of the 20th international conference on machine learning (ICML-03), pp. 856–863.

73. Center for International Earth Science Information Network - CIESIN - Columbia University, *Gridded Population of the World, Version 4 (GPWv4): Population Count*, `http://dx.doi.org/10.7927/H4X63JVC`, Accessed 30 November 2023, 2016.

74. E. A. Stuart *et al.*, Using propensity scores in difference-in-differences models to estimate the effects of a policy change. *Health Services and Outcomes Research Methodology* **14**, 166–182 (2014).

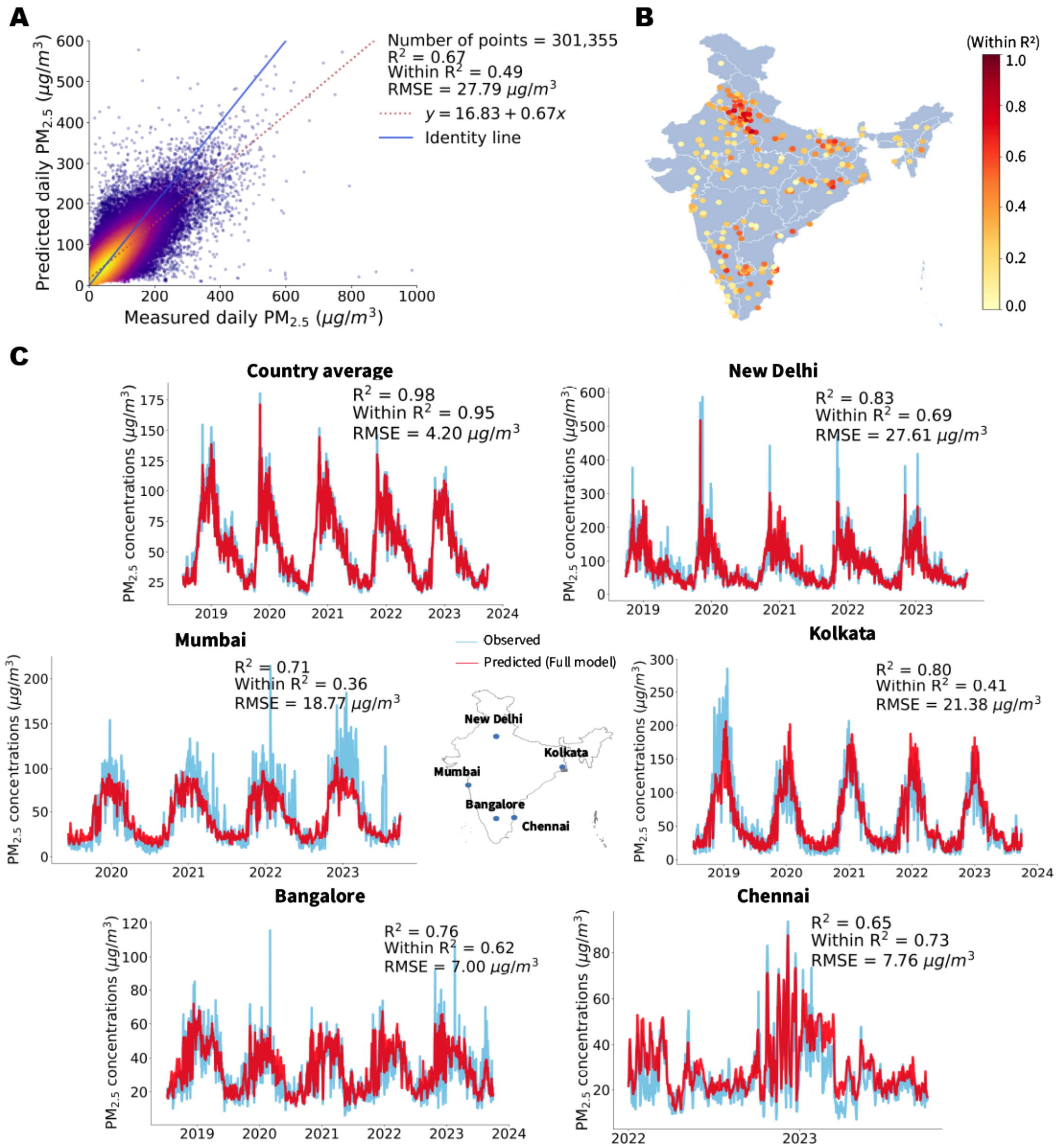

Figure 1: **Model performs well out-of-sample and across the range of observed $PM_{2.5}$ concentrations.** Panel A: the overall performance of the Full model. Colors indicate the count of monitor observations, with observed $PM_{2.5}$ on the horizontal axis and predicted $PM_{2.5}$ concentrations on the vertical axis. The blue line represents the 1–1 line, indicating perfect match between predictions and observations. Panel B: out-of-sample model performance in each grid cell with at least one monitor reporting on at least 5 days. Performance measured using "within R^2" after removing local seasonality and year trends. It is calculated over observed $PM_{2.5}$ using predicted $PM_{2.5}$ from the Full model in which that station was out-of-sample, with month of the year and year fixed effects. Panel C: the out-of-sample performance of the Full model in predicting daily time-series of observed $PM_{2.5}$ concentrations for the entire country, New Delhi, Mumbai, Bangalore, Chennai, and Kolkata. Different y-axis and x-axis scales are used in the figures to accommodate variations in $PM_{2.5}$ concentrations and monitor availability across the cities.

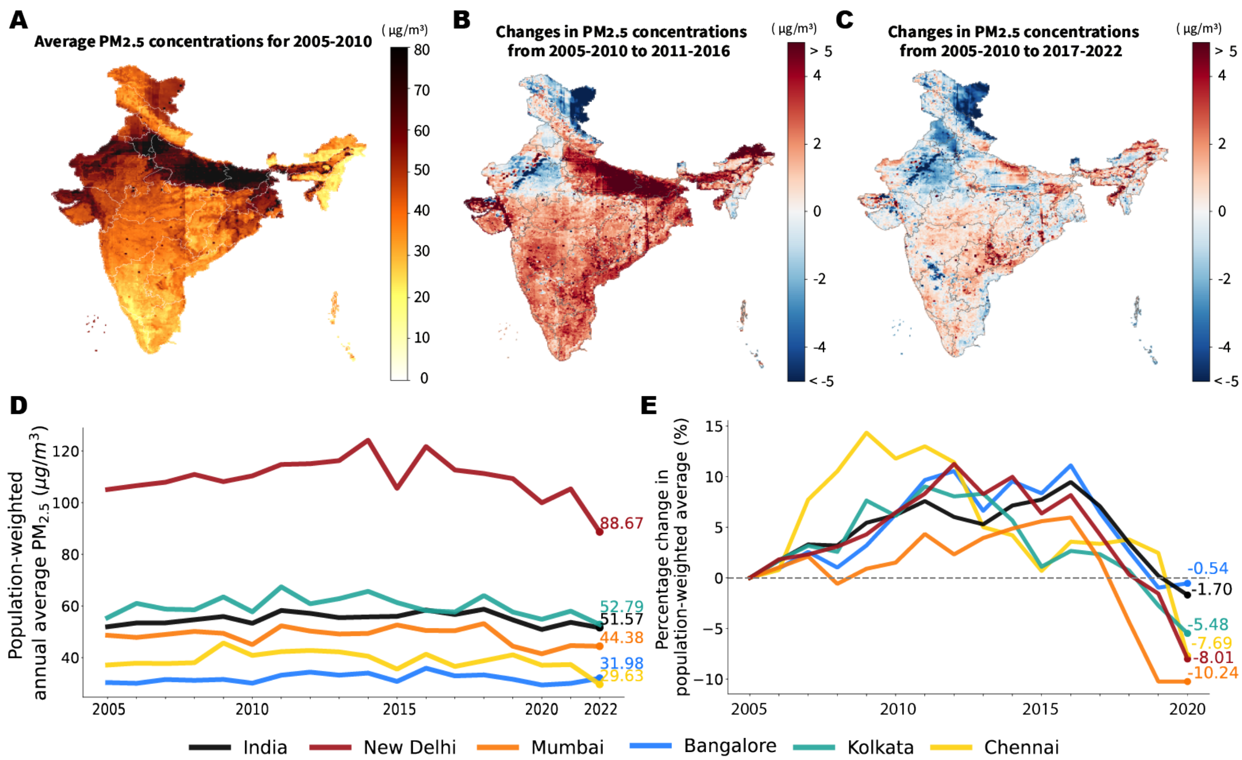

Figure 2: **$PM_{2.5}$ concentrations increased through 2016 but then declined through much of India thereafter.** Panel A: 6-year average $PM_{2.5}$ concentrations for 2005-2010 computed as the average over all days in each grid cell for 6 years. Panel B: changes in $PM_{2.5}$ concentrations between 2005-2010 and 2011-2016 show increases across most of the country. Panel C: changes in $PM_{2.5}$ concentrations between 2005-2010 and 2017-2022 show a mix of increases and declines. Panel D: population-weighted annual average $PM_{2.5}$ concentrations from 2005 to 2022, for all of India and selected mega-cities. Panel E: percentage changes in 3-year population-weighted averages relative to the 2005-2007 average, for all of India and selected mega-cities. The x-axis label represents the running means of years from 2005-2007 to 2020-2022.

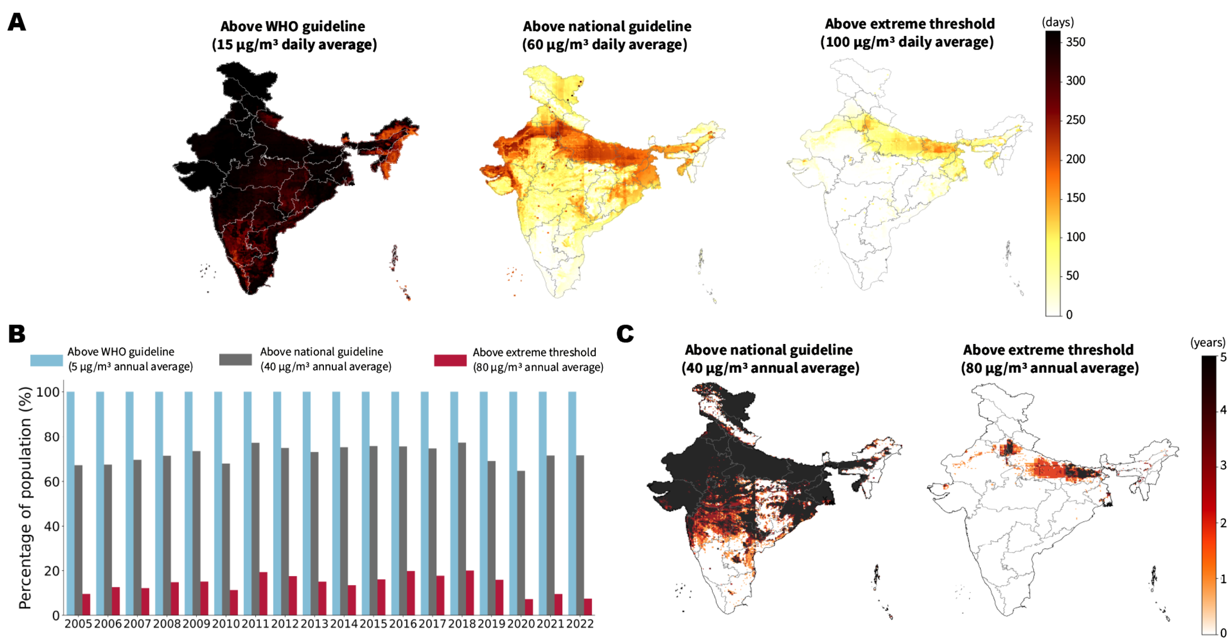

Figure 3: **Widespread exposure to elevated $PM_{2.5}$ concentrations across India, with daily extremes in the North.** Panel A: spatial distribution of grid cells with daily $PM_{2.5}$ concentrations above WHO guideline of 15 $\mu g/m^3$ (*53*) (left panel), national guideline of 60 $\mu g/m^3$ (center panel), and daily extreme threshold of 100 $\mu g/m^3$ (right panel), demonstrating the average number of days for each 10 km grid cell for 2018-2022. Panel B: proportion of populations exposed to annual averages of $PM_{2.5}$ concentrations exceeding WHO (5 $\mu g/m^3$) (*53*), national (40 $\mu g/m^3$), and extreme (80 $\mu g/m^3$) thresholds from 2005 to 2022. The entire population in India is consistently exposed to $PM_{2.5}$ concentrations above the WHO guideline during these years. Panel C: Locations highlighted in colors indicate areas where average $PM_{2.5}$ concentrations exceeded the national guideline of 40 $\mu g/m^3$ (left panel) and extreme threshold of 80 $\mu g/m^3$ (right panel) from 2018 to 2022, respectively. Colored gradients depict the number of years each grid cell exceeded each threshold during these years. The entire country would be shaded in colors on a map denoting the areas exposed to above the WHO threshold.

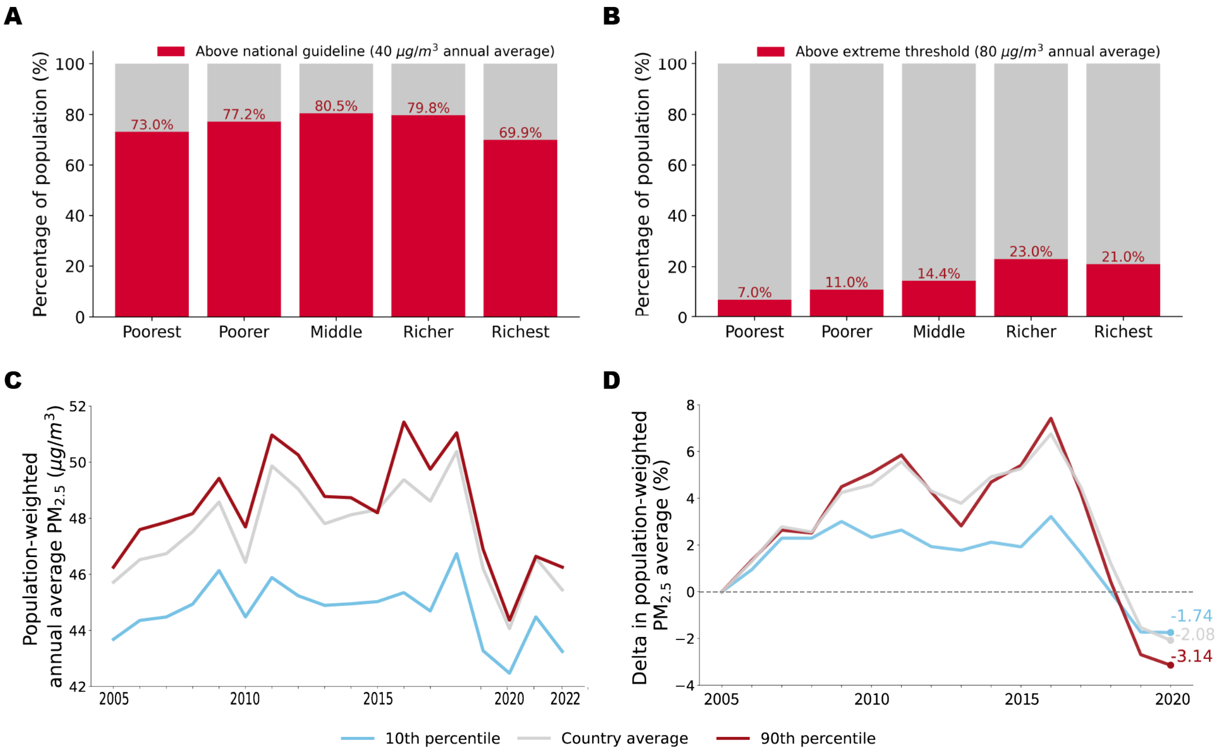

Figure 4: **Wealthier people experienced higher average $PM_{2.5}$ concentrations but faster recent declines.** Panel A: percentage of the population in each wealth category exposed to ambient $PM_{2.5}$ concentrations above the national guideline of 40 $\mu g/m^3$ for the years 2015-2019. These percentages were calculated using 5-year mean $PM_{2.5}$ concentrations from 2015 to 2019 because machine learning algorithms to generate wealth estimates (*54*) were trained on ground data from that period. Panel B: percentage of the population in each wealth category exposed to concentrations above the extreme threshold of 80 $\mu g/m^3$ for the years 2015-2019. Panel C: population-weighted annual average of $PM_{2.5}$ concentrations from 2005 to 2022 for the country average, locations with 90th percentile of wealth, and locations with 10th percentile of wealth. Panel D: percentage changes in 3-year population-weighted averages relative to the 2005-07 average. The x-axis label represents the running means of years from 2005-2007 to 2020-2022. Between 2020 and 2022, wealthier individuals experienced a 3.14% decline in PM2.5 exposure compared to the period of 2005-2007, while poorer individuals saw a 1.74% reduction. When compared to the period of 2015-2017, during which much of India began to experience an overall declining trend in PM2.5 concentrations, a wider disparity in reduction rates was observed, with the wealthiest experiencing an 8.11% reduction and the poorest experiencing a 3.60% reduction S23.

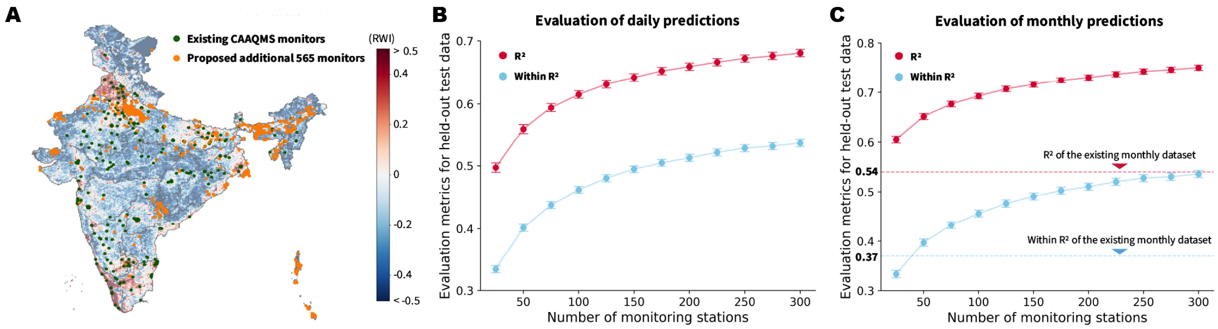

Figure 5: **Applications of our predictions for better air quality monitoring in India and other low- and middle-income countries.** Panel A: proposed locations of additional 565 CAAQMS identified by compressed sensing methods (see Materials and Methods), along with existing 435 monitor locations, ensuring increased equality in air quality monitoring across the country while capturing both baseline patterns and sudden anomaly spikes in $PM_{2.5}$ concentrations. Colored gradients indicate wealth estimates (Relative Wealth Indices (RWIs) (*54*)) in each grid cell. Panel B: model performance at a daily level as a function of number of stations used in training. Performance is measured by R^2 and "within R^2" as evaluated on a fixed number of held out stations (21 stations). Points represent the mean performance across 1,000 experiments (randomly re-sampling training and test sets) and whiskers denote the corresponding 95 % confidence intervals across experiments. Model performance increases with additional training data, but at a declining rate, with modest increases past 150 monitors. Panel C: model performance at a monthly level, estimated by aggregating the daily predictions and monitor data on a monthly basis. The dashed lines represent the R^2 and within R^2 values of the existing publicly-available monthly $PM_{2.5}$ dataset, evaluated against monitor data in India, which are 0.54 and 0.37, respectively.

Supplementary tables

Table S1: Input features used for the Full and AOD models.

Feature	Temporal scale	Source	Native resolution
TROPOMI NO_2*/**	daily, weekly rolling average	Sentinel-5P	1.11 km
TROPOMI CO*/**	daily, weekly rolling average	Sentinel-5P	1.11 km
AOD**	daily, weekly rolling average	MODIS MAIAC	1 km
AOT	daily, weekly rolling average	MERRA-2	50 km
CO (reanalysis data)	daily, weekly rolling average	MERRA-2	50 km
NO_2 (reanalysis data)	weekly rolling average***	OMI/Aura	25 km
Meteorology (temperature at 2 meters, dewpoint temperature at 2 meters, wind speed in the east ward and northward directions, total precipitation, net thermal radiation at the surface, surface pressure, relative humidity***, wind degree***)	daily, weekly rolling average	ECMWF ERA5	11.13 km
Land cover (water, shurub, urban, forest, savannas)	yearly	MODIS	500 meters
Land cover (low vegetation, high vegetation)	daily	ECMWF ERA5	11.13 km
Elevation	cross-sectional (as of 2000)	NASA SRTM	30 meters
Month and day of the year	daily	-	-
Binary variable indicating monsoon season (0 or 1)	daily	-	-
Latitude and longitude	cross-sectional	-	-
Percentage of missing observations in TROPOMI NO_2*, TROPOMI CO*, AOD	daily	-	-
Binary variables indicating whether each of TROPOMI NO_2*, TROPOMI CO*, AOD is imputed (0 or 1)	daily	-	-
Weighted TROPOMI NO_2* (NO_2 values multiplied by 1.0 for observations, 0.5 for imputed values)	daily	-	-
Weighted TROPOMI CO* (CO values multiplied by 1.0 for observations, 0.9 for imputed values)	daily	-	-
Weighted AOD (AOD values multiplied by 1.0 for observations, 0.8 for imputed values)	daily	-	-

*: Only included in the Full model.

**: Missing observations are imputed using machine learning methods before being incorporated into the model.

***: Calculated using the meteorological data derived from ECMWF ERA5.

****: Only weekly rolling average is computed and included due to the missing data in daily observations.

Table S2: Input features used for machine learning models for imputation of missing data in TROPOMI NO_2, TROPOMI CO, and AOD.

Feature	**Temporal scale**	**Source**	**Native resolution**
AOT	daily, weekly rolling average, annual average	MERRA-2	50 km
CO (reanalysis data)	daily, weekly rolling average, annual average, average of all days	MERRA-2	50 km
NO_2 (reanalysis data)	weekly rolling average, annual average**	OMI/Aura	25 km
Meteorology (temperature at 2 meters, dewpoint temperature at 2 meters, wind speed in the east ward and northward directions, total precipitation, net thermal radiation at the surface, surface pressure, relative humidity *, wind degree *)	daily, weekly rolling average, annual average	ECMWF ERA5	11.13 km
Land cover (water, shurub, urban, forest, savannas)	yearly	MODIS	500 meters
Land cover (low vegetation, high vegetation)	daily	ECMWF ERA5	11.13 km
Elevation	cross-sectional (as of 2000)	NASA SRTM	30 meters
Month, day of the year, cosine of day of the year	daily	-	-
Binary variable indicating monsoon season (0 or 1)	daily	-	-
Latitude and longitude	cross-sectional	-	-

*: Calculated using the meteorological data derived from ECMWF ERA5.

**: Only weekly rolling average and annual average are computed and included due to the missing data in daily observations.

Table S3: Hyperparameter ranges explored within inner 5-fold spatial CV using GridSearchCV for models imputing missing observations in TROPOMI NO_2, TROPOMI CO, and AOD.

Algorithm	**Hyperparameters**	**Range**
LightGBM	max_depth	3, 5, 8, 10, 15, 20
	learning_rate	0.01, 0.1
	num_iterations	500, 800, 1000, 1500, 3000
	num_leaves	800, 1000, 1500
	max_bin	255, 350, 500, 1000
	min_data_in_leaf	10, 20, 30, 40, 50
	lambda_l2	0, 1, 10, 100, 500
	boosting	gbdt
XGBoost	max_depth	3, 5, 8, 10, 15, 20
	learning_rate	0.01, 0.1
	gamma	0.2, 0.8, 1.0
	subsample	0.2, 0.8, 1.0
	min_child_weight	0.2, 0.8, 1.0
	n_estimators	500, 1000, 1500
	lambda	0, 1, 10, 100, 500
	booster	gbtree

Table S4: Optimal hyperparameters and corresponding out-of-sample predictive performances obtained through GridSearchCV using a 5-fold inner spatial CV for each model imputing missing observations in TROPOMI NO_2, TROPOMI CO, and AOD.

Model	**Algorithm**	**Hyperparameters**	**Results**
Imputation for missing TROPOMI NO_2	LightGBM	max_depth: 10	R^2: 0.50
		learning_rate: 0.1	RMSE: 1.82×10^{-5}
		num_iterations: 3000	
		num_leaves: 1500	
		max_bin: 500	
		min_data_in_leaf: 10	
		lambda_l2: 10	
		boosting: gbdt	
Imputation for missing TROPOMI CO	LightGBM	max_depth: 10	R^2: 0.92
		learning_rate: 0.1	RMSE: 0.003
		num_iterations: 3000	
		num_leaves: 1500	
		max_bin: 1000	
		min_data_in_leaf: 10	
		lambda_l2: 10	
		boosting: gbdt	
Imputation for missing AOD	XGBoost	max_depth: 20	R^2: 0.79
		learning_rate: 0.1	RMSE: 166.26
		gamma: 0.8	
		subsample: 0.8	
		min_child_weight: 1	
		n_estimators: 1000	
		lambda: 100	
		booster: gbtree	

Table S5: Out-of-sample performances of machine learning models for imputing missing observations in TROPOMI NO_2, TROPOMI CO, and AOD.

Model	**R^2**	**Within R^2**	**RMSE**	**Number of observations**
TROPOMI NO_2	0.52	0.27	2×10^{-5} (mol m^2)	934,138
TROPOMI CO	0.92	0.75	0.003 (mol m^2)	1,026,271
AOD (Full model)	0.82	0.76	155.21	965,224
AOD (AOD model)	0.82	0.75	147.23	1,264,830

Table S6: Hyperparameter ranges explored within inner 5-fold spatial CV using GridSearchCV for the Full and AOD models.

Algorithm	**Hyperparameters**	**Range**
LightGBM	max_depth	5, 8, 10, 15
	learning_rate	0.01, 0.1
	num_iterations	800, 1000, 1500
	num_leaves	800, 1023, 1500
	max_bin	255, 350, 500
	min_data_in_leaf	10, 20, 30, 40, 50
	lambda_l2	0, 1, 10, 100, 500
	boosting	gbdt
XGBoost	max_depth	5, 8, 10
	learning_rate	0.01, 0.1
	gamma	0.2, 0.8, 1.0
	subsample	0.2, 0.8, 1.0
	min_child_weight	0.2, 0.8, 1.0
	n_estimators	500, 1000, 1500
	lambda	0, 1, 10, 100, 500
	booster	gbtree

Table S7: Optimal hyperparameters and corresponding out-of-sample predictive performances obtained through GridSearchCV using a 5-fold inner spatial CV for the Full and AOD models.

Model	**Algorithm**	**Hyperparameters**	**Results**
Full model	XGBoost	max_depth: 10	R^2: 0.60
		learning_rate: 0.1	RMSE: 29.12
		gamma: 0.8	
		subsample: 0.8	
		min_child_weight: 0.8	
		n_estimators: 1500	
		lambda: 1	
		booster: gbtree	
AOD model	XGBoost	max_depth: 10	R^2: 0.60
		learning_rate: 0.1	RMSE: 29.37
		gamma: 0.8	
		subsample: 0.8	
		min_child_weight: 0.8	
		n_estimators: 1500	
		lambda: 1	
		booster: gbtree	

Supplementary figures

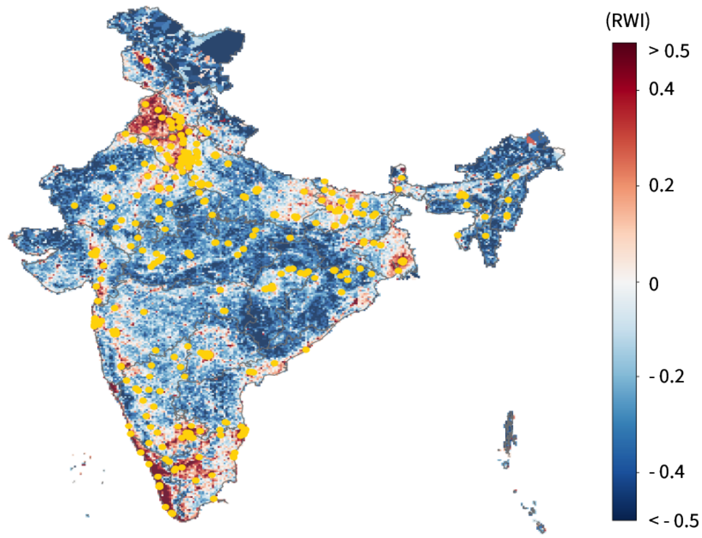

Figure S1: Location of CAAQMS monitors (n = 435) mapped with Relative Wealth Indices (*54*) (RWIs), which represent the relative wealth of each grid cell compared to others in the same country.

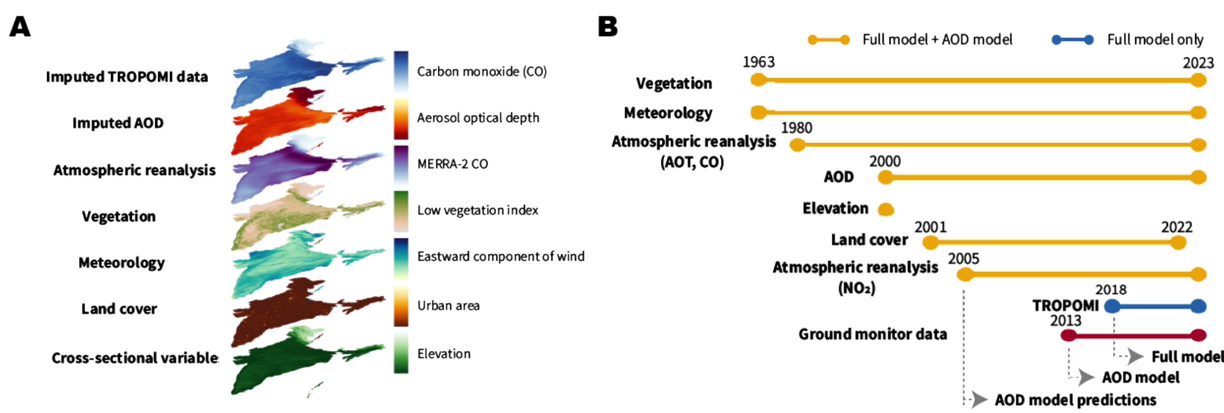

Figure S2: Panel A: input features utilized in the second-stage machine learning model predicting ambient $PM_{2.5}$ concentrations include both time-varying and cross-sectional variables. Gap-filled TROPOMI data are exclusively used for the Full model. Panel B: temporal availability of input features employed for the second-stage machine learning model. Due to the availability of TROPOMI data, the Full model is trained on ground monitor data from July 10, 2018, to September 30, 2023, and used to generate daily $PM_{2.5}$ predictions for the corresponding period. Additionally, the AOD model is trained from January 1, 2013, to September 30, 2023. The oldest availability of one of the input features, atmospheric reanalysis data (NO_2), allows the AOD model to generate $PM_{2.5}$ estimates from January 1, 2005, to September 30, 2023.

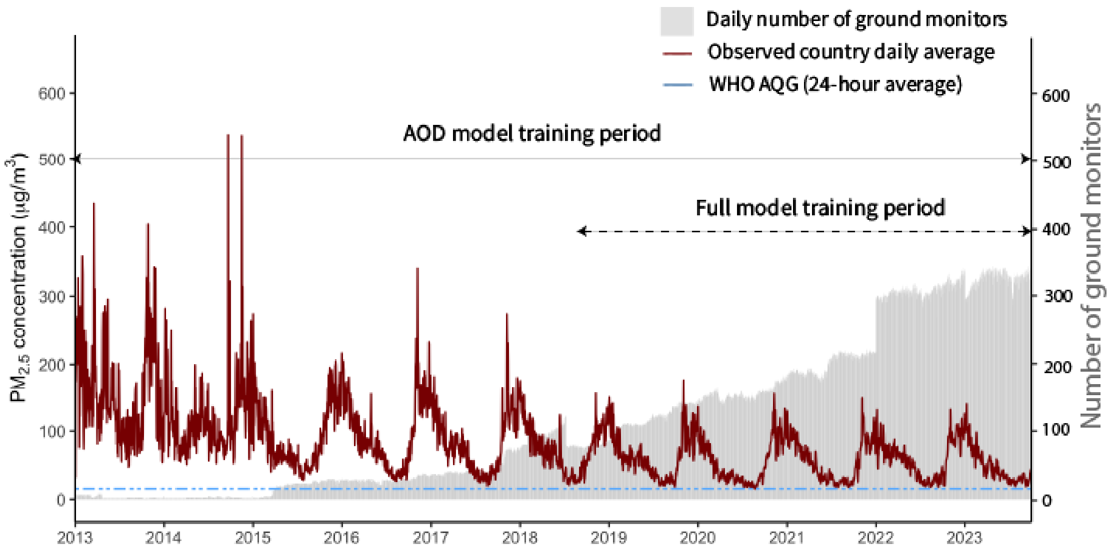

Figure S3: Daily country average of ground-measured $PM_{2.5}$ concentrations demonstrates a slightly declining trend over the decade; however, it remains at an endangering level, exceeding the 24-hour average of the World Health Organization (WHO) air quality guideline of 15 $\mu g/m^3$ (*53*). The number of air quality monitors has progressively increased over time, aligning with government efforts to expand the CAAQMS network. Two dashed lines represent the training periods for the Full and AOD models, respectively.

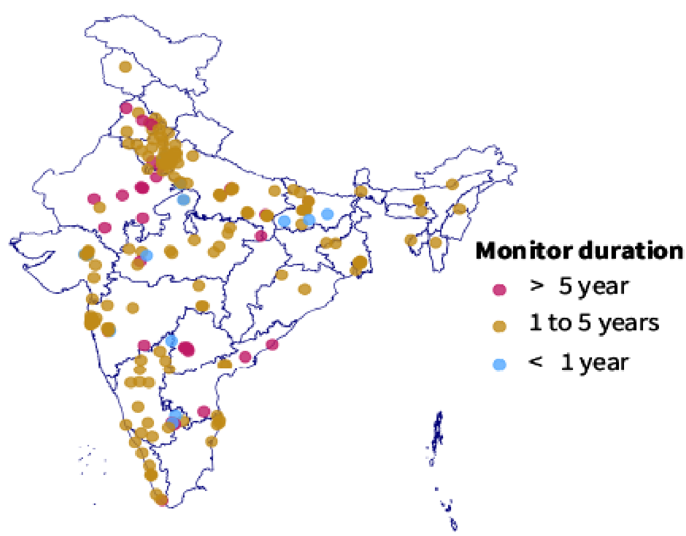

Figure S4: The location of 435 CAAQMS monitors used for this study, with data coverage ranging from less than 1 year to a maximum of 9 years of monitor data.

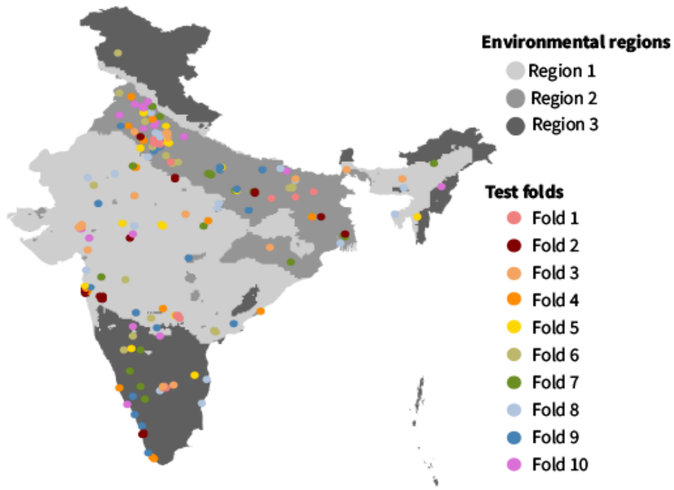

Figure S5: To balance environmental characteristics, such as urban versus rural areas, when splitting data into training and test sets using spatial 10-fold CV, three environmental regions are identified based on k-means clustering, utilizing imputed TROPOMI features, imputed AOD, and atmospheric reanalysis data. Each test fold includes a nearly equal number of 50 km blocks of 10 km grid cells from each of the three environmental regions. Each 50 km block of 10 km grid cells goes into only one of the 10 test folds.

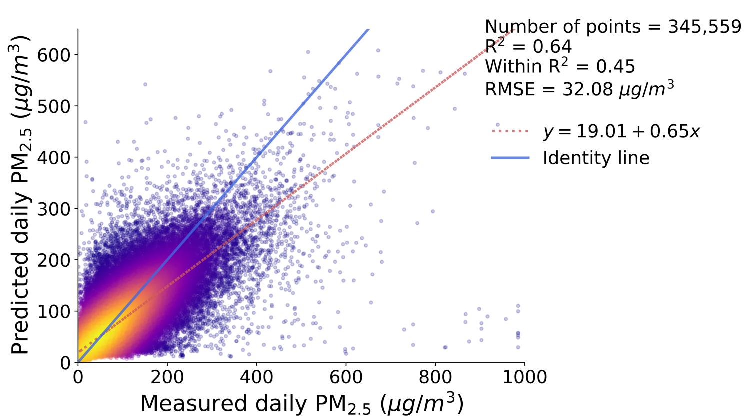

Figure S6: Performance evaluation of the AOD model, trained on $PM_{2.5}$ measurements from January 1, 2013, to September 30, 2023.

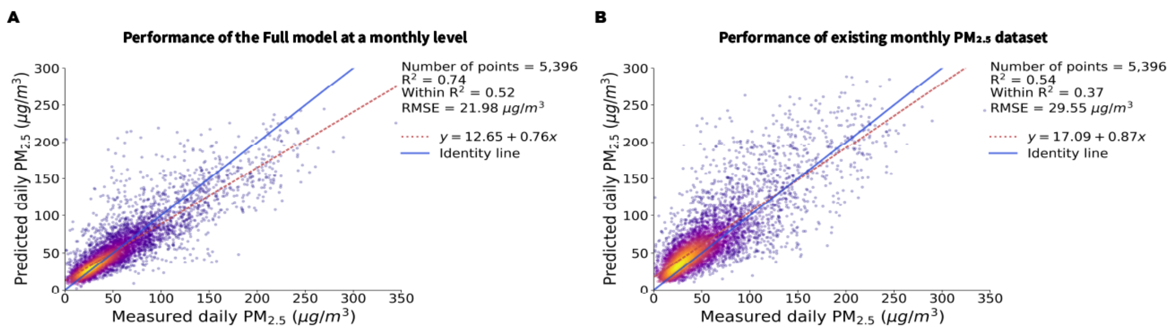

Figure S7: Panel A: monthly performance of the Full model using $PM_{2.5}$ daily observations and predictions aggregated at a monthly level from July 10, 2018, to December 31, 2021. Panel B: performance evaluation of the existing $PM_{2.5}$ monthly dataset (*14*), from July 2018, to December 2021, representing their latest available dataset, using the same monthly $PM_{2.5}$ observations as employed in the assessment of the Full model.

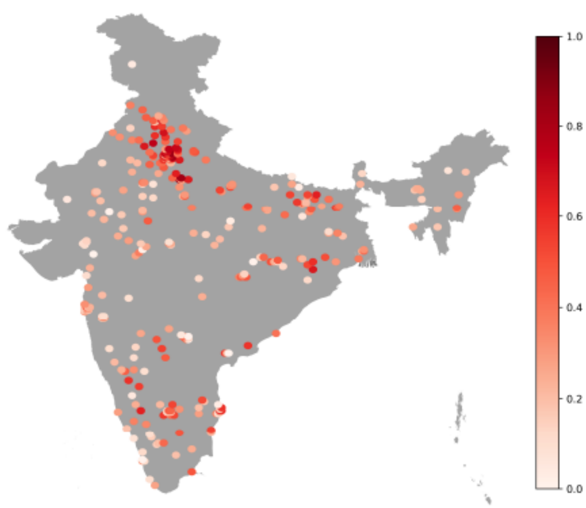

Figure S8: Out-of-sample within R^2 per 10 km by 10 km grid cell, calculated over $PM_{2.5}$ observations using $PM_{2.5}$ predictions derived from the AOD model for each location with at least 5 observations (points on map).

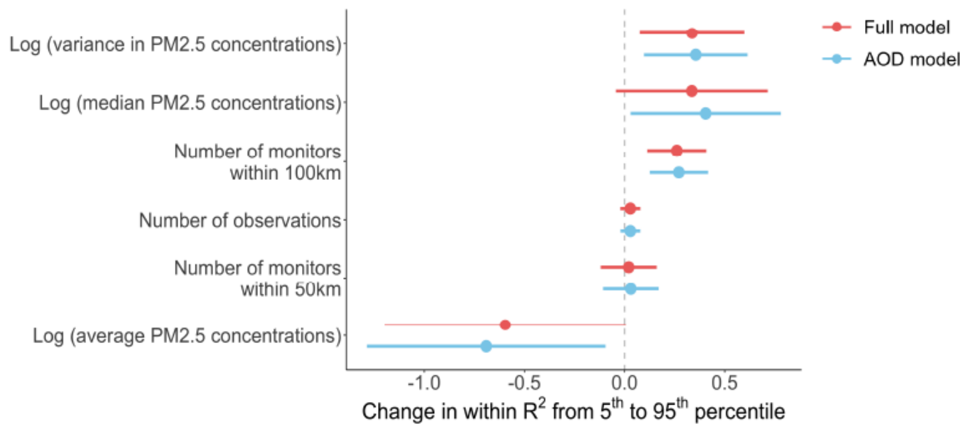

Figure S9: Linear regression results relating monitor-specific performance (within R^2) shown in (Fig 1B)) to location characteristics. Predictive power of each characteristic is calculated as the estimated change in monitor within R^2 when each characteristic is increased from the 5th to 95th percentile of its distribution. Points show central estimates, and line segments show 95% confidence intervals.

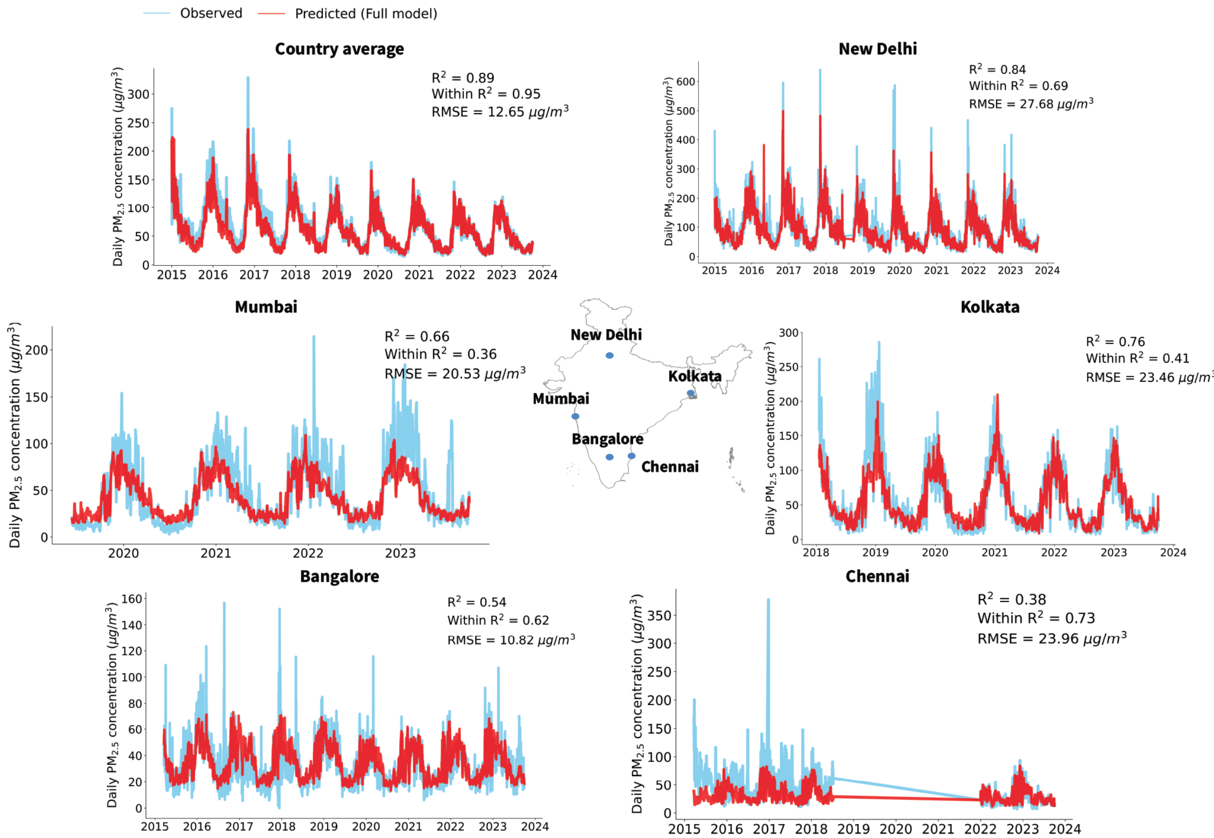

Figure S10: Temporal performance of the AOD model across five mega-cities. Different y-axis and x-axis scales are used in the figures to accommodate variations in $PM_{2.5}$ concentrations and monitor availability across the cities. No monitor data is available for Chennai from July 2018 to December 2022.

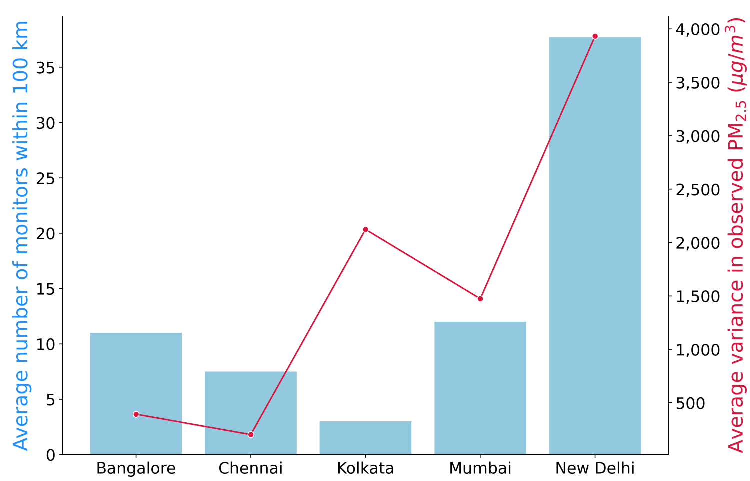

Figure S11: Average number of air quality monitors within 100 km and average variance in observed $PM_{2.5}$ concentrations in each city.

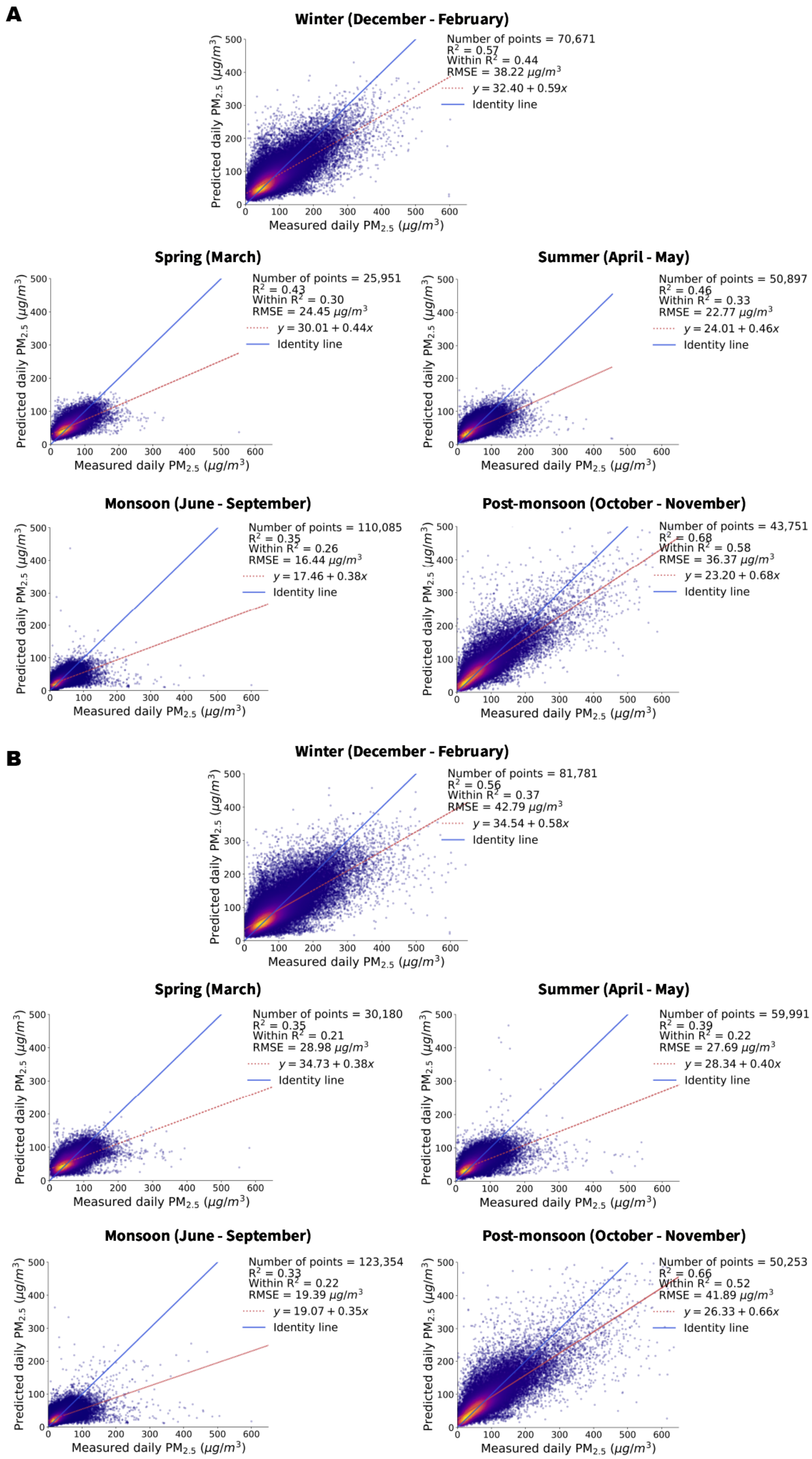

Figure S12: Panel A: seasonal performances of the Full model. Panel B: seasonal performances of the AOD model.

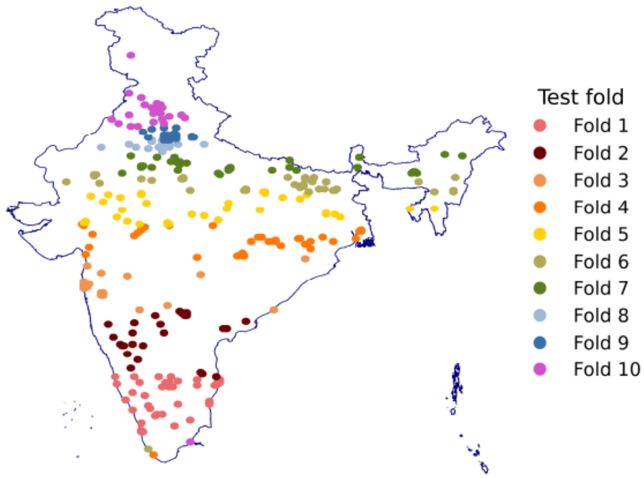

Figure S13: Locations of test data based on latitude included in each of the 10 test folds.

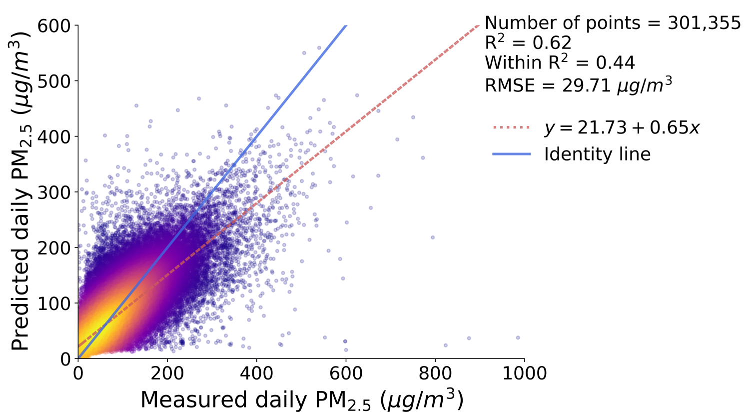

Figure S14: Performance evaluation of the Full model using larger blocks of test data based on latitude.

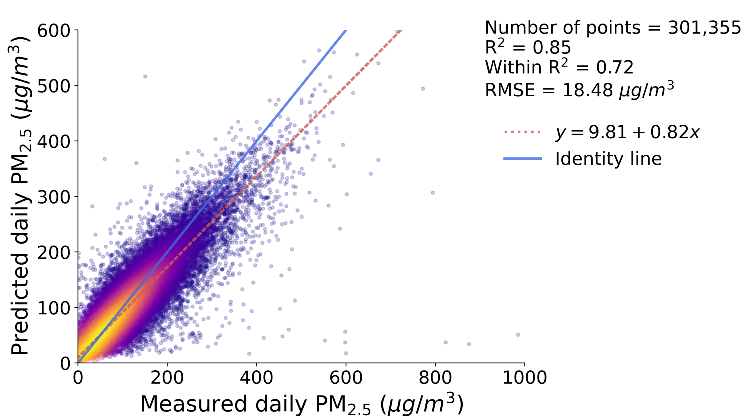

Figure S15: Performance evaluation of the Full model using random 10-fold CV.

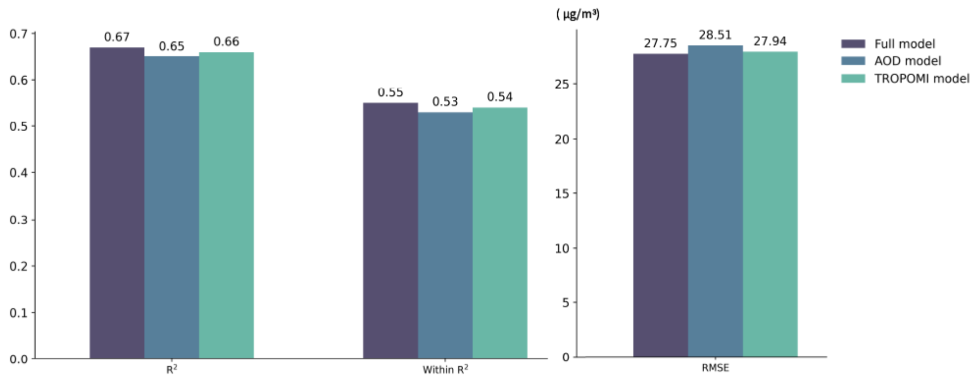

Figure S16: Out-of-sample performances of the Full, AOD, and TROPOMI models using the same sets of training and test data from July 10, 2018, to September 30, 2023.

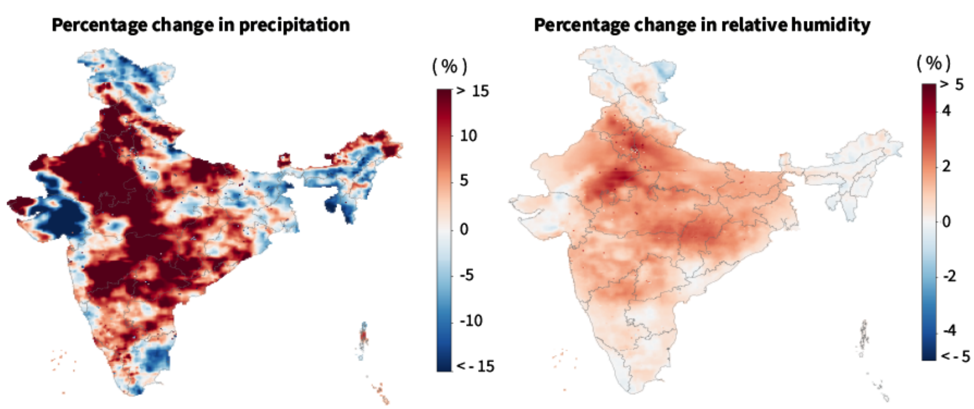

Figure S17: Percentage change in precipitation (left panel) and relative humidity (right panel) calculated for each 10 km grid from 2005-2015 to 2016-2022 using daily total precipitation, temperature, and dewpoint temperature obtained from ECMWF ERA5 data. Temperature and dewpoint temperature are utilized to compute relative humidity for each 10 km grid.

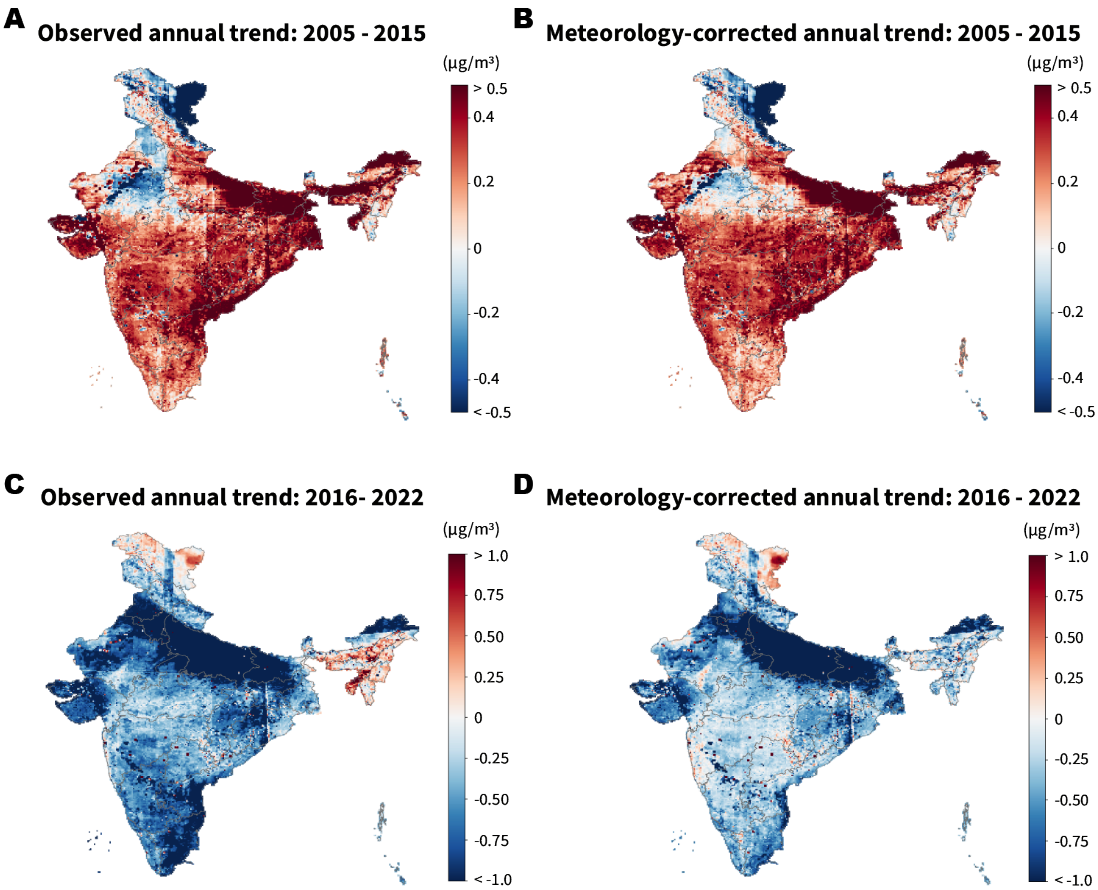

Figure S18: Panel A: average annual trend of observed $PM_{2.5}$ from 2005 to 2015. Panel B: average annual trend of $PM_{2.5}$ concentrations after controlling for local meteorology from 2005 to 2015. Panel C: average annual trend of observed $PM_{2.5}$ from 2016 to 2022. Panel D: average annual trend of $PM_{2.5}$ concentrations after controlling for local meteorology from 2016 to 2022.

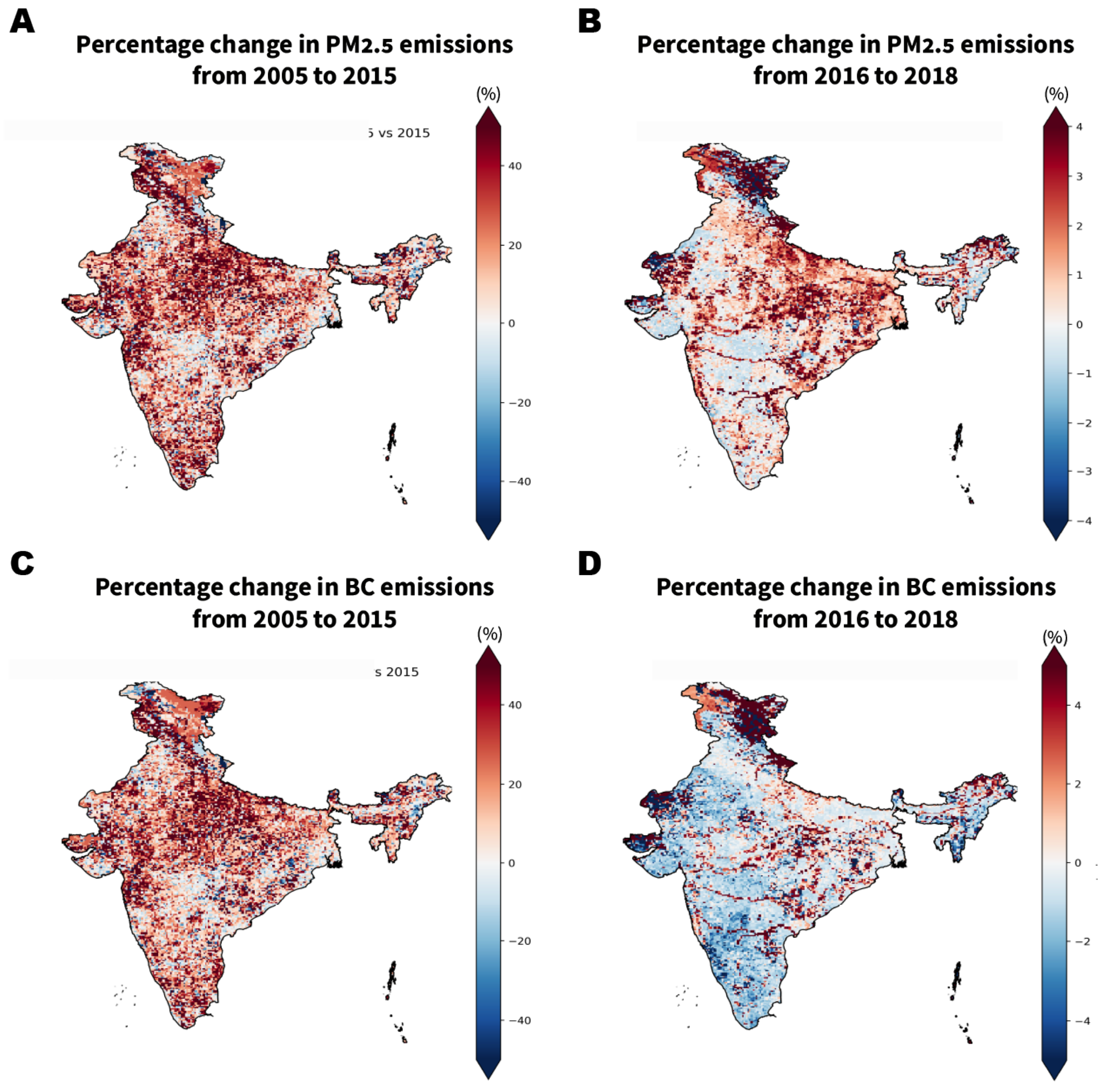

Figure S19: Panel A: percentage change in $PM_{2.5}$ emissions from 2005 to 2015. Panel B: percentage change in $PM_{2.5}$ emissions from 2016 to 2018. Panel C: percentage change in BC emissions from 2005 to 2015. Panel D: percentage change in BC emissions from 2016 to 2018.

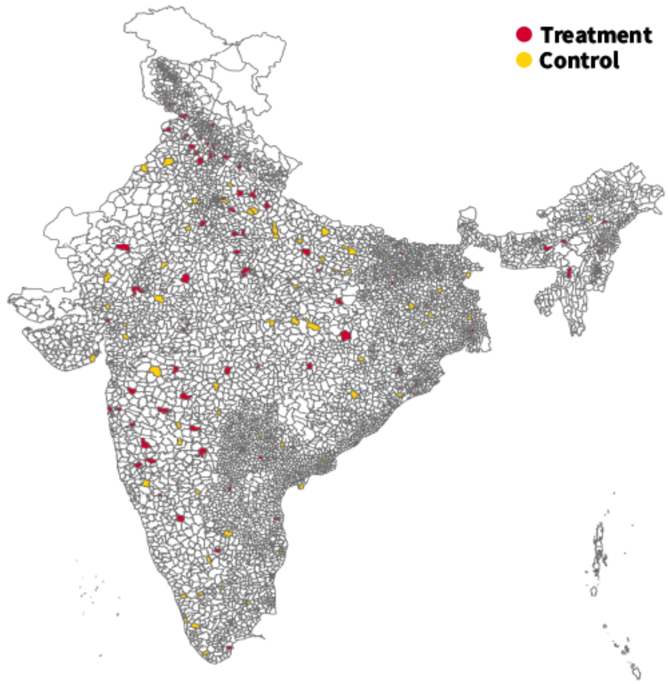

Figure S20: 88 treatment subdistricts consisting of NCAP's 102 non-attainment cities whose clean action plans were approved in 2020, along with 74 control subdistricts selected using a propensity score method. To account for spillover effects, control subdistricts are not adjacent to treatment subdistricts and located outside a 50 km radius from them.

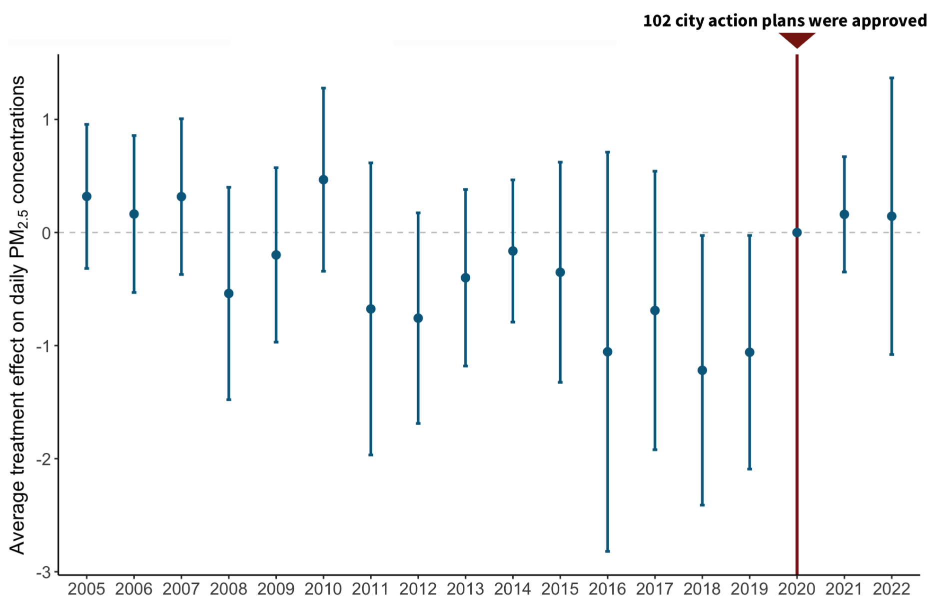

Figure S21: Average changes in daily $PM_{2.5}$ concentrations post the implementation of NCAP do not show a statistically significant difference between treatment and control subdistricts, highlighting that there is no evidence that NCAP contributed to declines in the $PM_{2.5}$ concentrations.

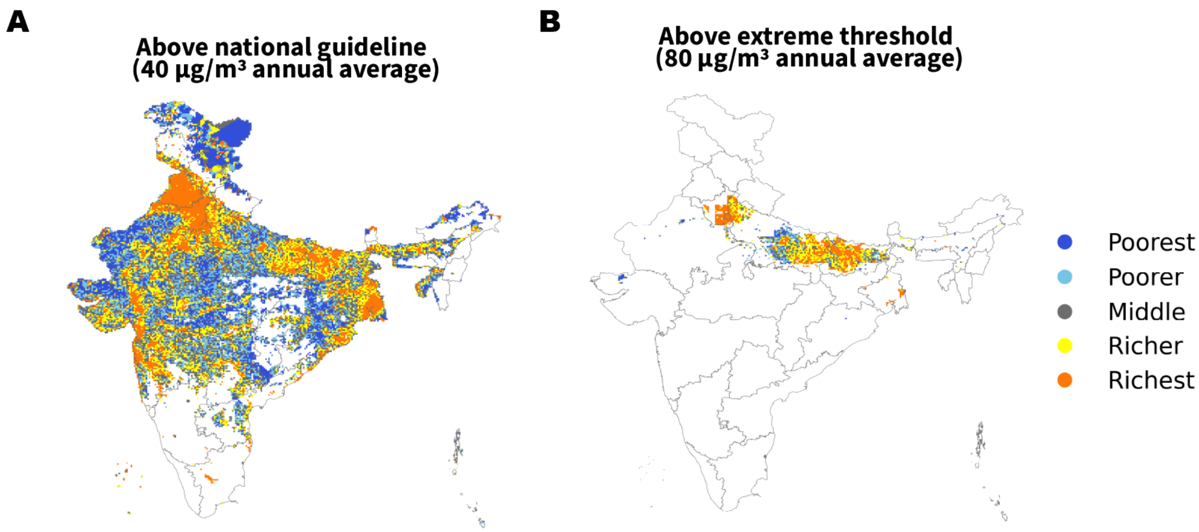

Figure S22: Panel A: locations that were exposed to average concentrations of $PM_{2.5}$ exceeding the national guideline of 40 $\mu g/m^3$ per wealth category during 2015-2019. Panel B locations with $PM_{2.5}$ average concentrations above the extreme threshold of 80 $\mu g/m^3$ per wealth category during the same period.

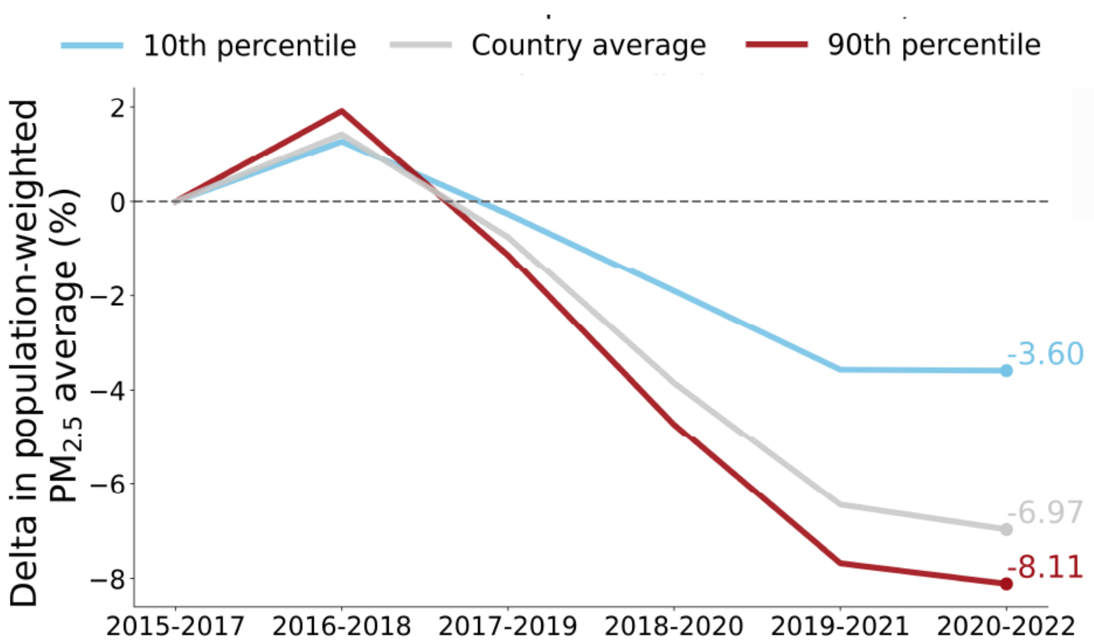

Figure S23: Percentage changes in 3-year population-weighted averages relative to the 2015-17 average. The x-axis label represents the running means of years from 2015-2017 to 2020-2022.

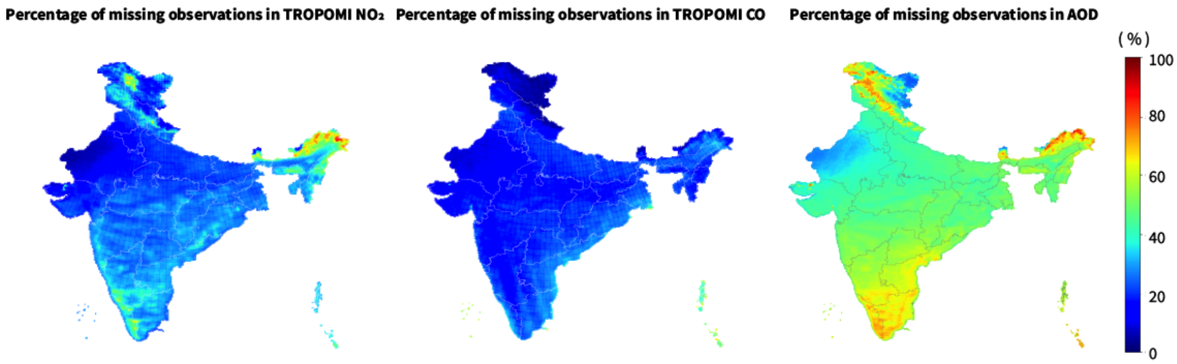

Figure S24: Percentage of daily observations missing in TROPOMI NO_2, TROPOMI CO, and MODIS AOD data per 10 km grid from July 10, 2018, to September 30, 2023.

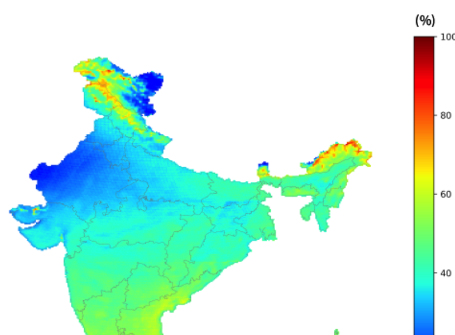

Figure S25: Percentage of daily observations missing in MODIS AOD data per 10 km grid from January 1, 2013, to September 30, 2023.